MEMORANDUM
RESEARCH DEPARTMENT

To: HR, HO, HMD, HMOS, RD staff and consultants

Copy: D

From: Jean Bidlot, Peter Janssen and Saleh Abdalla

Date: April 7, 2005 File: R60.9/JB/0516

Subject: A revised formulation for ocean wave dissipation in CY29R1.

Abstract

The wave model dissipation source function has been reformulated in terms of a mean steepness parameter and a mean frequency that give more emphasis on the high-frequency part of the spectrum and results in a more realistic interaction between windsea and swell. This has allowed the relaxation of the prognostic frequency range over which the model equations are integrated. A few other small adjustments were also necessary to take adavantage of the increased dynamic range of the model. This revised formulation of the model has resulted in improved analyses of wave model parameters, particularly those that are most sensitive to the high frequency part of the spectrum.

1 Introduction.

In the ECMWF version of the wave model WAM (ECWAM), dissipation due to white-capping, S_{ds}, is modelled in the manner suggested by Hasselmann (1974).

Introduce the mean frequency $\langle\omega\rangle$ by means of the inverse mean frequency,

$$\langle\omega\rangle = \int d\vec{k}\ F(\vec{k}) / \int d\vec{k}\ F(\vec{k})/\omega \tag{1}$$

with $F(\vec{k})$ the wavenumber spectrum, $\vec{k}$ the wavenumber and ω the angular frequency. A similar relation for the mean wavenumber $\langle k \rangle$ is

$$\sqrt{\langle k \rangle} = \int d\vec{k}\ F(\vec{k}) / \int d\vec{k}\ F(\vec{k})/\sqrt{k}. \tag{2}$$

Hasselmann (1974) suggested the following dissipation source function

$$S_{ds} = -\gamma_d F, \tag{3}$$

with

$$\gamma_d = \beta \langle \omega \rangle\ s^{2m} \left[(1-a)\frac{k}{\langle k \rangle} + a\left(\frac{k}{\langle k \rangle}\right)^2 \right], \tag{4}$$

where the mean steepness s is defined as

$$s^2 = \langle k \rangle^2 \int d\vec{k}\ F(\vec{k}) \tag{5}$$

Here, β, a and m are constants which still need to be determined. It is remarked that in the original work of Hasselmann (1974) the second term in the square bracket is absent. The reason for this is that Hasselmann assumed a large separation between the length scale of the waves and the whitecaps, giving a power 1 for the wavenumber in the dissipation term. For the high-frequency part of the wave spectrum, however, such a large gap between waves and whitecaps may not exist, therefore allowing the possibility of a different dependence of dissipation on wavenumber.

The first rationale attempt to determine the unknown coefficients in the dissipation source function was reported by Komen et al. (1984). These authors started from the empirical expression for wind input of Snyder et al. (1981), which was adapted to accomodate friction velocity scaling, whilst the exact form of Hasselmann's nonlinear transfer was taken. For a constant wind speed, the energy balance equation was integrated until stationary conditions were reached, and the unknown coefficients m and β were chosen in such a way that the equilibrium spectrum resembled the Pierson-Moskovitz (1964) spectrum as closely as possible (Note that in their work a was put to zero from the outset). The power m was found to be equal to 2 while the coefficient β was of the order of 3.

Later, Janssen introduced a wind input source function based on Miles theory, which resulted in much higher inputs at higher frequencies (Komen et al. 1994). Consequently, the dissipation source function required some adaptation, in particular at higher frequencies. He fixed m to 2 and he found, using the DIA approximation to the nonlinear transfer, optimal results for $a = 0.5$ and $\beta = 4.5$.

In this note, it is shown why the ECWAM formulation of the dissipation due to whitecapping is not entirely adequate when both windsea and low frequency swell are present. Namely, the mean steepness and mean frequency parameters used in the parametrisation of the dissipation are too much determined by the swell rather than by the windsea part of the spectrum. Together with a relaxation of the prognostic frequency range over which the model equations are integrated, a new definition for the characteristic mean parameters is suggested that is less sensitive to the presence of low frequency swell. A few other fine tuning modifications were also necessary as described in section 2. Simple examples on how the revised formulation compares to the old one are given in section 3. The new configuration of the model was tested both in stand-alone mode and in the coupled configuration. A summary of the results is presented in section 4.

2 Revised formulation.

In this new version of ECWAM, wave dissipation due to whitecapping, S_{ds}, is still modelled in the manner suggested by Hasselmann (1974). However, the mean steepness s and mean frequency $\langle\omega\rangle$ are defined using weighted spectral integrals that put more emphasis on the high frequencies.

Introduce the mean angular frequency $\langle\omega\rangle$ by means of the first ω-moment,

$$\langle\omega\rangle = \int d\vec{k}\ \omega F(\vec{k}) / \int d\vec{k}\ F(\vec{k}) \tag{6}$$

with $F(\vec{k})$ the wavenumber spectrum, $\vec{k}$ the wavenumber and ω the angular frequency. A similar relation for the mean wavenumber $\langle k\rangle$ is also used,

$$\sqrt{\langle k\rangle} = \int d\vec{k}\ \sqrt{k} F(\vec{k}) / \int d\vec{k}\ F(\vec{k}) \tag{7}$$

then defining the mean steepness s as in (5)

The dissipation source function is still modelled as

$$S_{ds} = -\gamma_d F, \tag{8}$$

with

$$\gamma_d = \beta\langle\omega\rangle\ s^4\ \left[(1-a)\frac{k}{\langle k\rangle} + a\left(\frac{k}{\langle k\rangle}\right)^2\right], \tag{9}$$

where β and a are two contant parameters to be determined.

Another point of concern is the choice of the maximum value of the prognostic frequency range. For frequencies above this maximum frequency, ECWAM enforces a diagnostic f^{-5} spectral shape. Since July 1999 the ECWAM model defines this prognostic range as all frequencies f which satisfy

$$f \leq \min(2.5 f_{mean}, f_{max}) \tag{10}$$

where f_{max} is the maximum discretised frequency ($f_{max} \simeq 0.41 Hz$ for 25 frequencies and 0.54 Hz for 30 frequencies) and $f_{mean} = \langle\omega\rangle/2\pi$. It replaced the previous definition of the original WAM cycle 4 (WAMcy4), where the upper prognostic frequency was given by

$\min(\max(2.5 f_{mean}, 4 f_{PM}), f_{max})$ (with f_{PM} the Pierson-Moskovitz frequency). Back then, this change had a favourable impact on relations such as the mean square slope versus wind speed while, compared to ERS-2 altimeter wave height data, the first-guess wave height error reduced by 5%. However, under light wind conditions in the presence of low-frequency swell, it is very likely that no windsea is generated. Although this is a relatively minor problem in terms of global wave height statisitcs, it will affect verification statistics for the mean period as pointed out by Kumar et al. (2003) and by Oceanor near the coast of India, Steve Barstow private communication, and from our own verification against 1-D buoy wave spectra (Janssen 2004). Therefore, it would be desirable to introduce a more flexible prognostic frequency range to capture windseas in light wind situations. However, this should be done in such a way that relations such as mean square slope and Charnock parameter versus wind speed do not suffer. Similarly, the choice of this upper limit should not be influenced by the presence of low frequency swell. In CY29R1, we have substituted in Eq.(10) the mean frequency of the total sea by the mean frequency of the wind sea only f_{meanWS}. Namely,

$$f \leq \min(2.5 f_{meanWS}, f_{max}) \tag{11}$$

where f_{meanWS} is the mean frequency based on the ω^{-1} moment (Eq.(1)) but only for spectral components that satisfy

$$S_{input} > 0. \quad or \quad \frac{28}{c}\, u_* \, \cos(\Delta\theta) \geq 1. \tag{12}$$

where S_{input} is the wind input source term, c is the phase speed, u_* is the friction velocity and $\Delta\theta$ is the difference between the wind direction and the wave propagation direction.

A tuning exercise was performed in such a way that the duration limited growth curve for significant wave height and the time evolution of the Charnock parameter resembled as much as possible the corresponding results of the reference model (which is essentially WAMcy4, but using Eq. (10).

As a result we found that

$$\beta = 2.1, \; a = 0.6, \text{ and } \hat{\alpha} = 0.0095 \tag{13}$$

where $\hat{\alpha}$, is a constant that controls the asymptotic value of the Charnock parameter α.

$$\alpha = \hat{\alpha}/\sqrt{1 - \tau_w/\tau} \tag{14}$$

where τ is the total stress and τ_w the wave induced stress.

A few other small adjustments were also necessary. By analysing simple wave growth cases, we found that for light winds the Hersbach-Janssen limiter (1999) to the wave growth was not sufficiently controlling the growth (i.e there were signs of unstable growth). It was reduced by a factor of 0.6 (COEF4=3x 10^{-7}) and f_{mean} was also substituted with f_{meanWS} to remove the dependence of the limiter on the presence of low frequency swell.

Finally, it had been known for a while that more accurate results could be obtained if the total stress table that relates the wind speed and the wave induced stress τ_w was expressed in terms of $\sqrt{\tau}_w$ instead of τ_w. This was however never implemented in the operational version of ECWAM before CY29R1.

3 Results for simple configurations.

In Fig. 1 the wave height evolution for the new model is compared to the reference run over a 10-day period in the context of the one grid point model with constant wind forcing of 15 m/s. The resemblance is satisfactory, but it cannot be perfect for the following reasons: for short times the growth limiter is more effective in the new model configuration resulting in less fast growth, and, because of the new steepness definition the new set up shows a slightly faster growth before levelling off to similar level at saturation for long times. For large winds the saturation in wave height only plays a role for very large duration, hence it is expected that extreme sea states will be enhanced by this change. This may be a different story for light wind cases where saturation already occurs in one day.

Fig. 2 displays the time evolution of the Charnock parameter. The parameter $\hat{\alpha}$ has been chosen in such a way that for large times there is agreement between new set up and reference run.

In the next experiment swell decay is compared. The one grid point model was run for 2 days with a constant wind of 15 m/s, after which the windspeed dropped to 5 m/s while the wind direction turned by 90°. Results for wave height are shown in Fig. 3. Decay time scales in the new setup are slightly longer because the dissipation source function is a more sensitive function of the sea state.

The final set of experiments were performed with the aim to investigate the impact of the presence of low-frequency swell on the growth of windsea. The swell spectrum was imposed at 90° to the right of the wind direction spectrum with a peak frequency of $0.045 Hz$. For a windspeed of $10 m/s$ Fig. 4 shows what happens according to the old model configuration. At first, with the definition of prognostic range given in Eq. (10) no

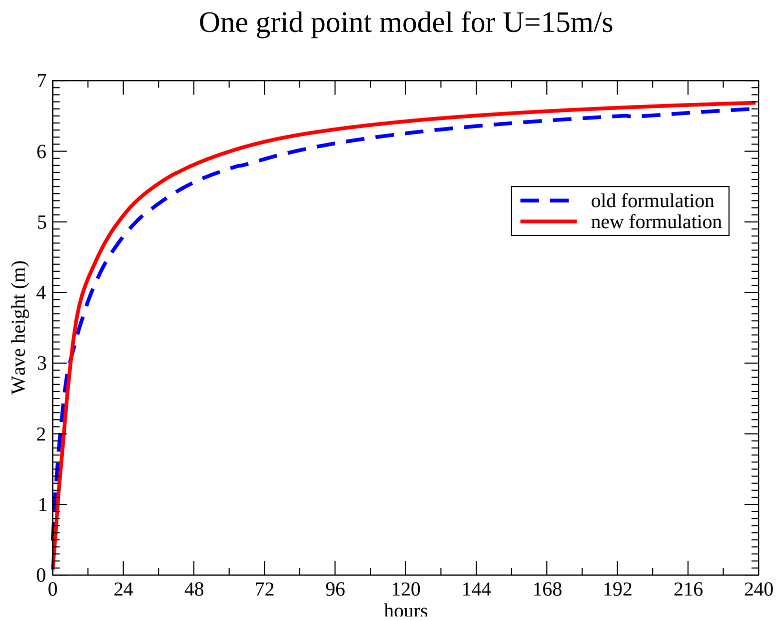

Figure 1: Time evolution of wave height for the one grid point model over a 10-day period when forced by constant 15 m/s wind. The integration time step is 900 s.

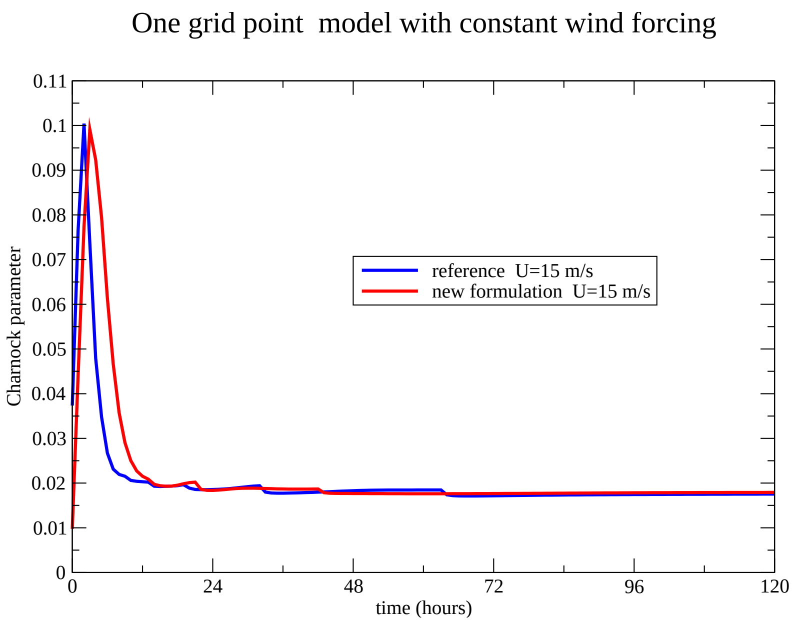

Figure 2: Time evolution of the Charnock parameter over a 10-day period. The wind speed is 15 m/s. The parameter $\hat{\alpha}$ has been chosen in such a way that for large times there is agreement between new set up and reference run. The integration time step is 900 s.

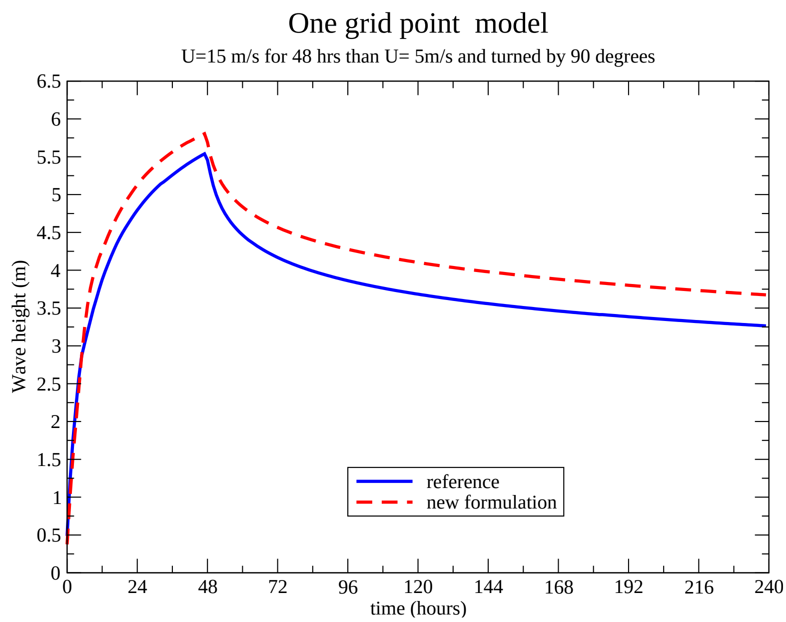

Figure 3: Time evolution of significant wave height over a 10-day period. Initially the wind speed is 15 m/s, and after 48 hrs it drops to 5 m/s while the wind direction turns by 90°.

windsea is generated (not shown), while with the wider frequency range of the original WAMcy4 windsea is generated but it does not grow as fast as without swell (panel a). This behaviour was found to be connected to the old growth limiter as expressed using f_{mean}. In the presence of swell, f_{mean} is reduced and the limiter becomes too strict, preventing the initial growth of the windsea. Substituting f_{mean} with f_{meanWS} in the new formulation of the limiter removes this dependency. At later stage, after the initial first few hours, the windsea in the presence of swell becomes much larger than in the absence of swell. This was however not the intention of the original WAM development. The reason for the too large windsea in the presence of swell is in the old (CY28R3) definition of the mean wave steepness which gives a considerable emphasis on the low frequencies. For the new formulation, with Eq. (11) instead, the results for the interaction of windsea and swell are shown in Fig. 5. The new setup now gives a satisfactory qualitative behaviour of the interaction of windsea and swell since the windsea grows at almost the same rate with or without the presence of swell.

4 Real case assesement.

4.1 stand-alone WAM.

The initial testing of the new formulation was done in the context of stand-alone WAM hindcasts. In this configuration, WAM is forced by 6-hourly analysed 10m winds and no wave data are assimilated. An example of the impact of the new formulation in terms of the mean difference (new-old) for significant wave height (H_s) and zero-crossing mean period (T_z) for a boreal winter (Dec. 2003) is shown in Fig. 6 and another example during a northern hemisphere summer is shown in Fig. 7 (July 2004). Areas with substantial differences are apparent, especially for T_z. With the new formulation, wave heights are larger in the storm tracks, whereas they are less in the tropics. Mean periods are much reduced, in particular around India, and both in the eastern tropical Pacific and Atlantic. These areas are usually dominated by swell but also under the influence of short-fetch winds or subject to relatively low winds. These conditions are better modelled by the new formulation. A similar situation is also visible for the northern hemisphere summer (Fig. 7), except that during summer months the north Pacific is also dominated by swell accompanied with short fetch/duration storms and some reduction in wave height occurs.

These hindcasts were compared to all available wave observations. A global comparison with altimeter wave heights from ENVISAT and Jason is presented in Table 1. For all ocean basins combined, there is a reduction in scatter index for both seasons with little change to the global bias, still slightly negative. In the tropics, the scatter index is also nicely reduced with a global bias that becomes negative. It is interesting to analyse how the model bias is distributed geographically. In winter (Fig. 8), the model has a tendency to overestimate wave heights in the eastern tropical Pacific. The new formulation reduces this positive bias, however for the whole of the tropics, it does not diminish the underestimation that is otherwise prevalent on the western side of the ocean basin as well as in the north equatorial counter current region (between 0° and 10°N), resulting

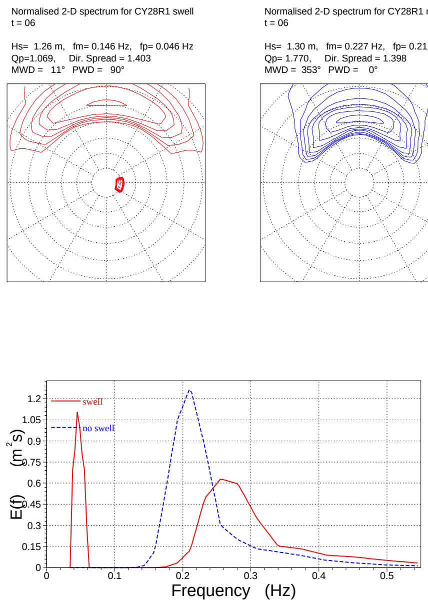

(a) t= 6

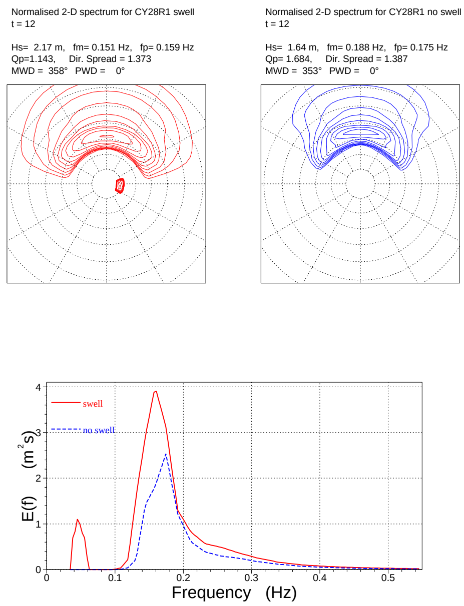

(b) t=12

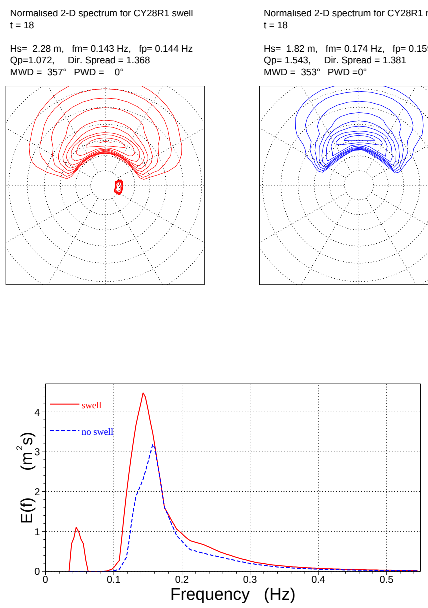

(c) t=18

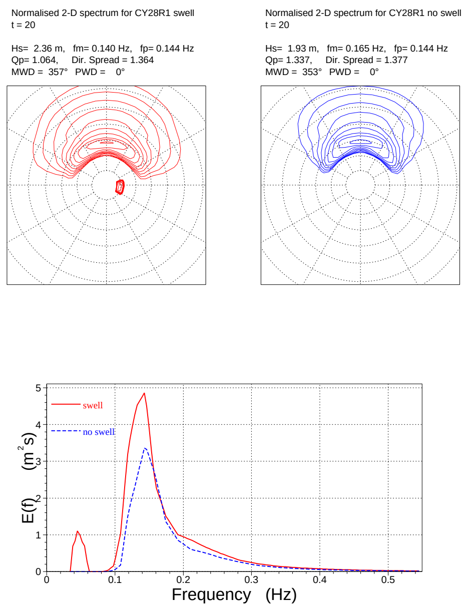

(d) t=24

Figure 4: Time evolution of one grid point model 2-d and 1-d spectra in the presence of swell (in red) or not (in blue) for CY28R1 with the upper prognostic frequency of the original WAMcy4 ($\min(\max(2.5f_{mean}, 4f_{PM}), f_{max})$). In the presence of such swell, the default CY28R1 setup does not give any growth of windsea and is not shown. The wind speed is constant at 10 m/s. The spectra are shown every 6 hours for a day from the start. For each time, the 2-d spectra are plotted using the same 10 contour levels that are chosen between the minimum and the maximum values of both cases. The concentric circles are spaced every 0.1 Hz.

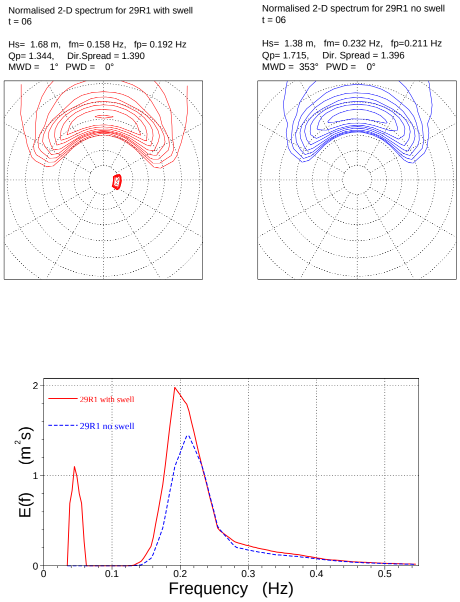

(a) t= 6

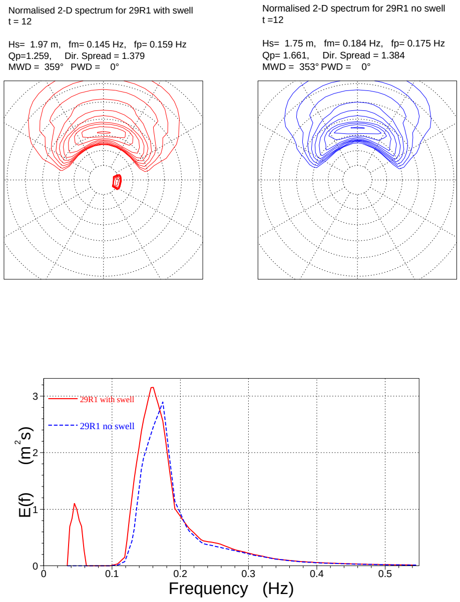

(b) t=12

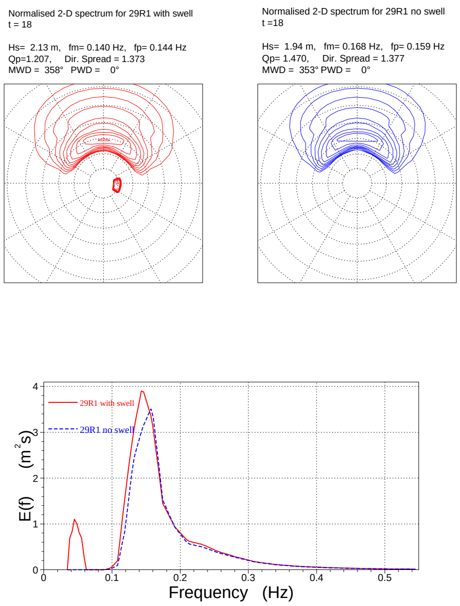

(c) t=18

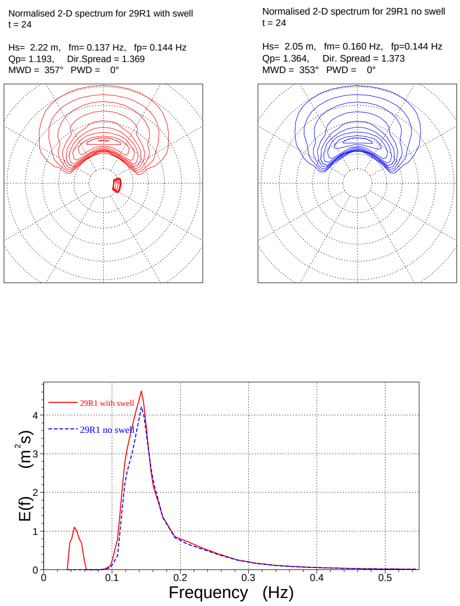

(d) t=24

Figure 5: Time evolution of one grid point model 2-d and 1-d spectra in the presence of swell (in red) or not (in blue) for CY29R1. The wind speed is constant at 10 m/s. The spectra are shown every 6 hours for a day from the start. For each time, the 2-d spectra are plotted using the same 10 contour levels that are chosen between the minimum and the maximum values of both cases. The concentric circles are spaced every 0.1 Hz.

in an overall negative bias in the tropics. The understimation in the counter equatorial current is not yet fully understood but it is possibly connected to the lack of wave current interaction in the present system. The increase in wave height in the storm tracks in both hemispheres seems to be in better agreement with the data except for areas near the ice edge in the southern ocean. There is a known problem with wave height overestimation near the Antartica ice edge. The new formulation does not address this problem and since it has a tendency to be more active in these areas, it makes the situation worse. In summer (Fig. 9), the northeastern Pacific also suffers from a systematic overestimation in wave height. The new formulation however appears to have reduced the error as was the case with the winter period except again near the southern ice edge.

Comparison with altimeter wave heights - S.I.(%) [bias(m)]				
data source	old (winter)	new (winter)	old (summer)	new (summer)
ENVISAT global	15.28 [-0.05]	14.43 [-0.04]	13.75 [-0.08]	13.29 [-0.08]
Jason global	16.37 [-0.07]	15.31 [-0.05]	14.77 [-0.08]	13.91 [-0.07]
ENVISAT tropics	14.66 [0.01]	13.75 [-0.04]	12.31 [-0.04]	11.80 [-0.09]
Jason tropics	15.59 [0.01]	14.61 [-0.04]	13.52 [0.01]	13.11 [-0.05]

Table 1: Comparison of the stand-alone 0.5° WAM hindcasts with altimeter wave heights for December 2003 (winter) and July 2004 (summer). No data assimilation was performed for the hindcasts. Operational analysis winds were used to force WAM. The old formulation (old) is compared to the new one (new) in terms of scatter index (standard deviation of the difference normalised by the mean of the observations) and bias (model-altimeter). Both quality controlled ENVISAT and Jason data were reduced by 4% and were averaged over the model grid. Tropics are defined as the area between $\pm 20°$.

Buoy and platform wave data can also be used for the comparison. The coverage is not global and mainly representative of northern hemisphere coastal areas, but the advantage is that the comparison can also be made in terms of wave periods. Table 2 confirms the improvement in terms of wave heights but also shows the marked gain in terms of mean wave period. There is however a slight deterioration in the peak period.

A good insight into the nature of this under/over estimation can be obtained by comparing the wave model spectra with buoy 1-D spectra. This study is however limited to the American and Canadian coastal areas, including Hawaii (with the exception of Christmas Island in the equatorial Pacific). Nevertheless, this comparison (Fig. 10) indicates that the old formulation underestimates wave energy at high frequency (the windsea part of the spectrum). This is still true if the buoy network is split per ocean basin. For winter months, the underestimation is also present at all frequencies. For summer months, the model largely overestimates swell at around 12 seconds (this is most pronounced in the northeastern Pacific). As expected, the new formulation does indeed improve the prediction of windsea and also reduces the swell overestimation of the summer months at around 12 seconds. Note however, that it does not improve the model fit to the data for very long period swell (above 18 sec.). Further analysis indicates that there are still

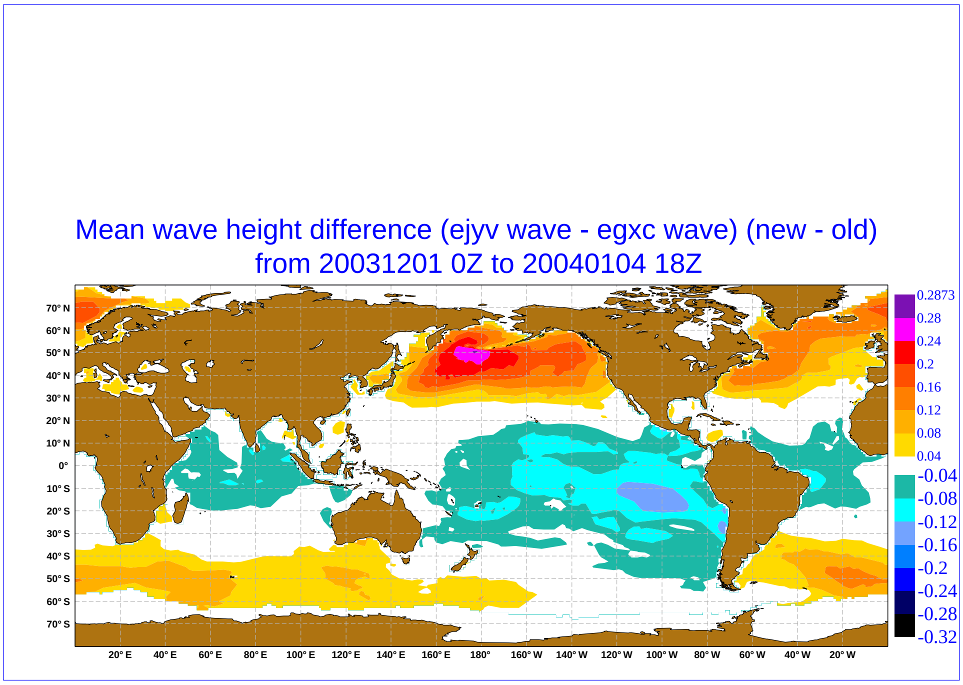

(a) wave height

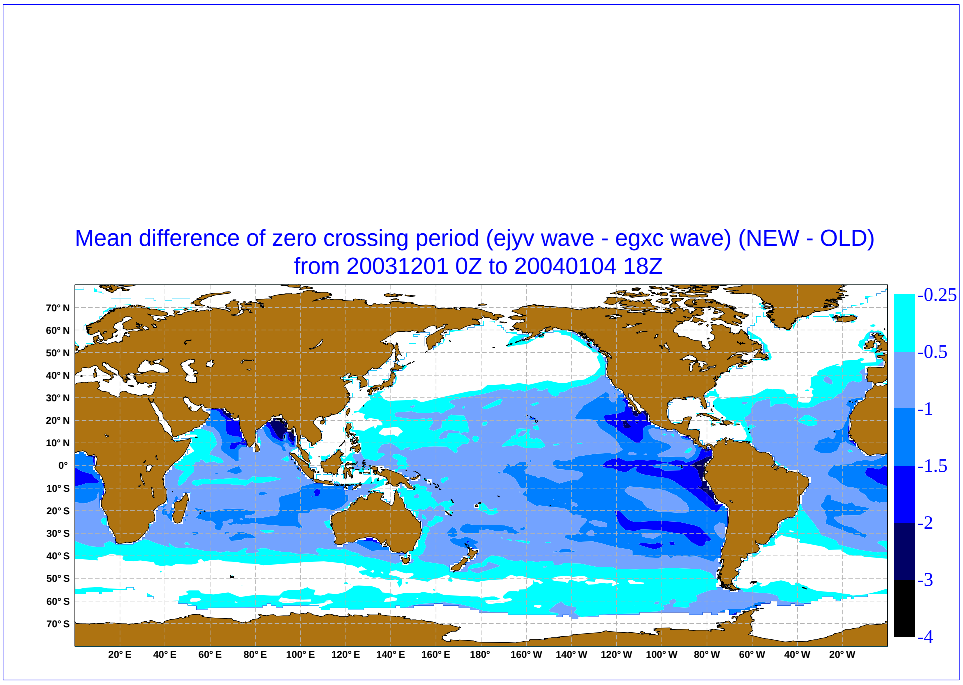

(b) mean period

Figure 6: Mean difference (new-old) for December 2003 for stand-alone 0.5° WAM hindcasts without any data assimilation. Colour shading is only used if the absolute difference is larger than 4 cm for wave heights and 0.25 sec. for mean periods.

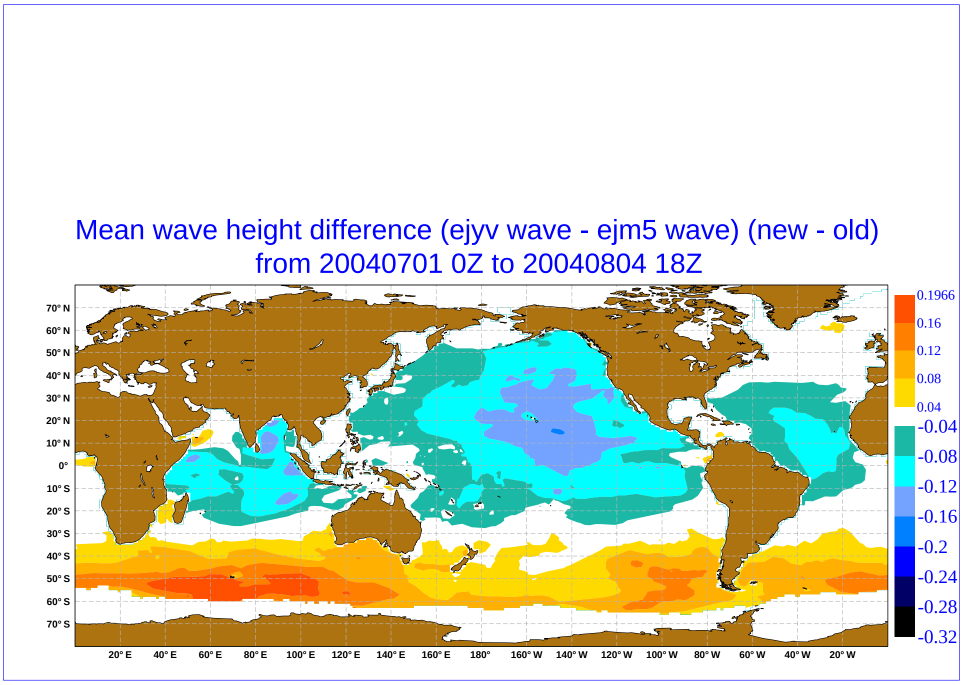

(a) wave height

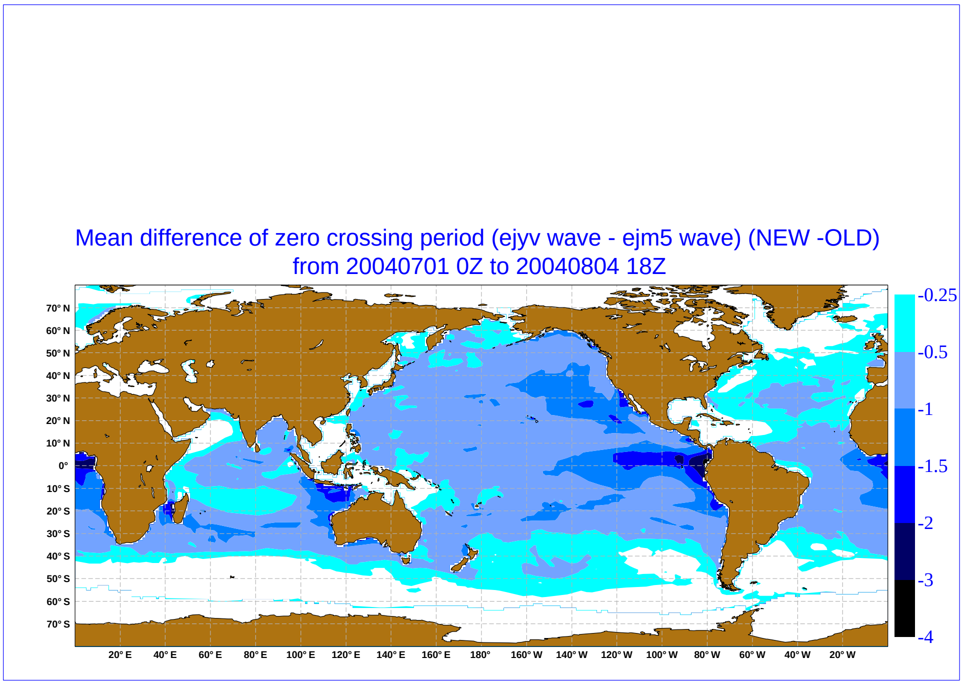

(b) mean period

Figure 7: Mean difference (new-old) for July 2004 for stand-alone 0.5° WAM hindcasts without any data assimilation. Colour shading is only used if the absolute difference is larger than 4 cm for wave heights and 0.25 sec. for mean periods.

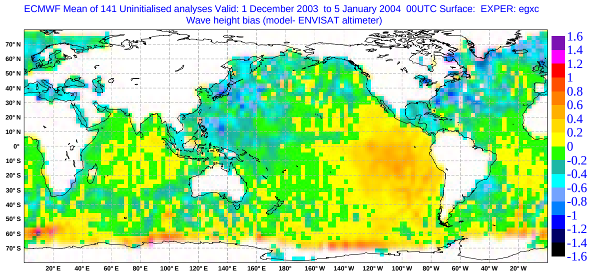

(a) old - ENVISAT

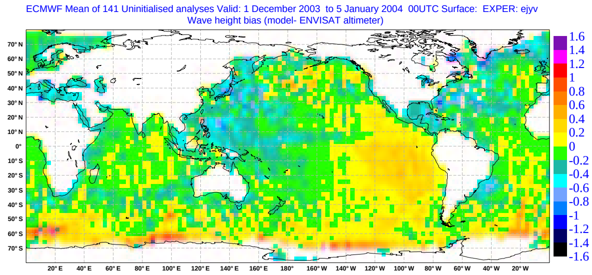

(b) new - ENVISAT

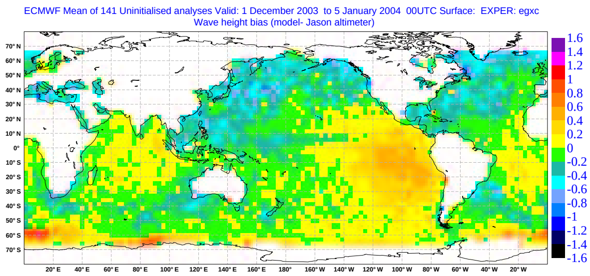

(c) old - Jason

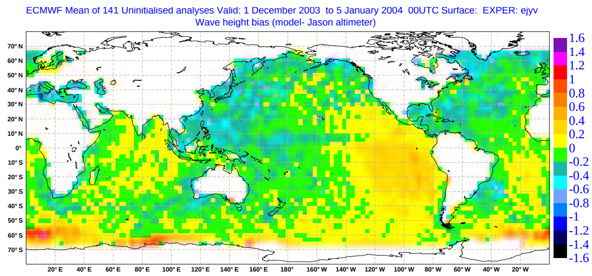

(d) new - Jason

Figure 8: Mean difference between model hindcast and altimeter wave heights for a period from December 1st 2003 to January 5th 2004 as presented in Table 1. Gridded altimeter data and model values were averaged over 3°x3° grid boxes. Two top panels are for ENVISAT and the two bottom panels for Jason.

Comparison with buoy data - S.I.(%) [bias (m or s)]				
data source	old (winter)	new (winter)	old (summer)	new (summer)
H_s GTS all	17.56 [-0.36]	16.54 [-0.28]	21.88 [0.01]	20.48 [-0.02]
T_p GTS US/Can	16.41 [-0.22]	16.87 [-0.05]	29.04 [0.57]	30.99 [0.63]
T_z 1-D US/Can	12.41 [0.25]	9.94 [0.03]	17.05 [0.69]	11.04 [0.17]
T_z GTS Europe	10.08 [-0.10]	9.00 [-0.29]	10.37 [-0.01]	10.22 [-0.17]

Table 2: Comparison of the stand-alone 0.5° WAM hindcasts with buoy data for December 2003 (winter) and July 2004 (summer). No data assimilation was performed for the hindcasts. Operational analysis winds were used to force WAM. The old formulation (old) is compared to the new one (new) in terms of scatter index (standard deviation of the difference normalised by the mean of the observations) and bias (model-buoy) for wave height (H_s), peak period (T_p) and mean period (T_z). The buoy data were either obtained from the operational archive (GTS) or derived from 1D buoy spectra obtained via the web from the U.S. National Data Buoy Center (NDBC) and the Canadian Marine Environmental Data Service (MEDS). The comparison is presented either for all selected locations (all) or locations along the American and Canadian coasts (US/Can) or buoys around Iceland and the British Isles (Europe).

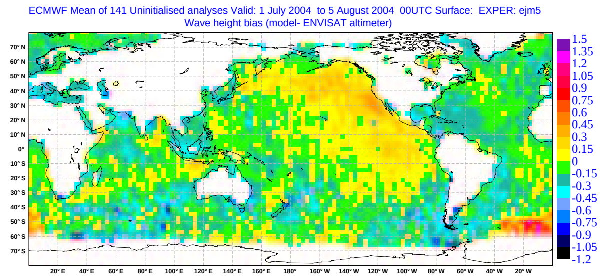

(a) old - ENVISAT

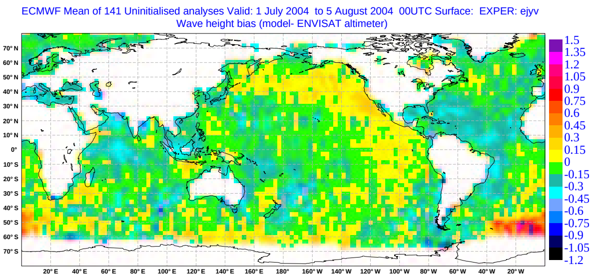

(b) new - ENVISAT

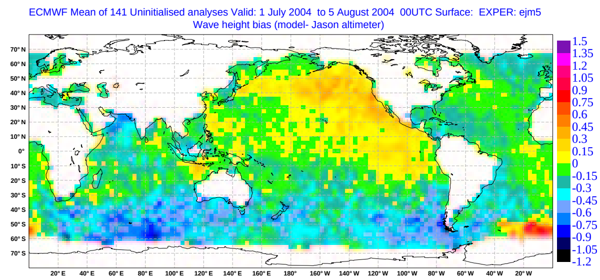

(c) old - Jason

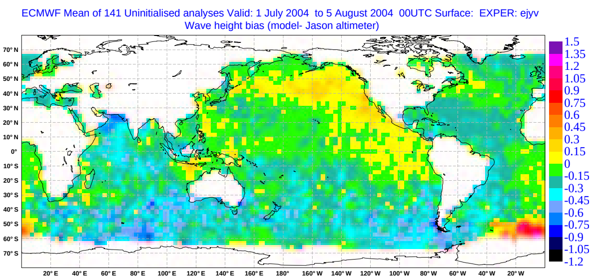

(d) new - Jason

Figure 9: Mean difference between model hindcast and altimeter wave heights for a period from July 1st 2004 to August 5th 2004 as presented in Table 1. Gridded altimeter data and model values were averaged over 3°x3° grid boxes. Two top panels are for ENVISAT and the two bottom panels for Jason.

cases when low frequency swell is present in the model but not in the data. Moreover, by comparing the arrival time of those swell events between model and a given buoy indicates that the model swell usually arrives sooner and lasts longer than observed. This is indicative of too much diffusion in the model. The advection scheme in WAM is known to be quite diffusive, more work is needed to test other suitable advective schemes to see if they can improve the prediction of low frequency swell.

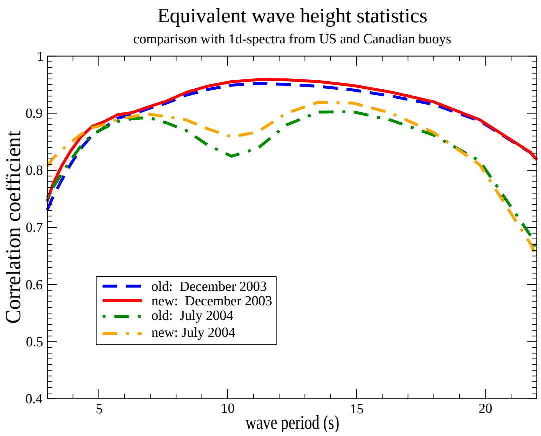

(a) correlation coefficient

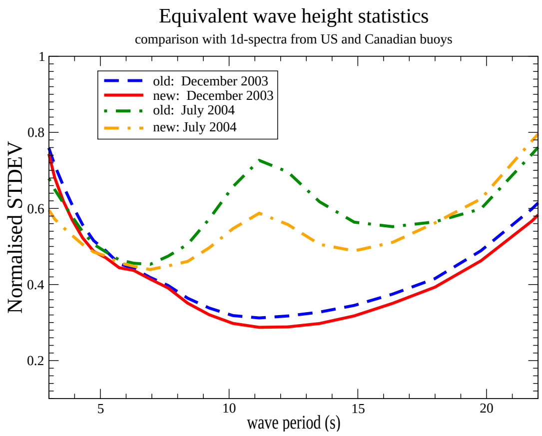

(b) normalised STDEV

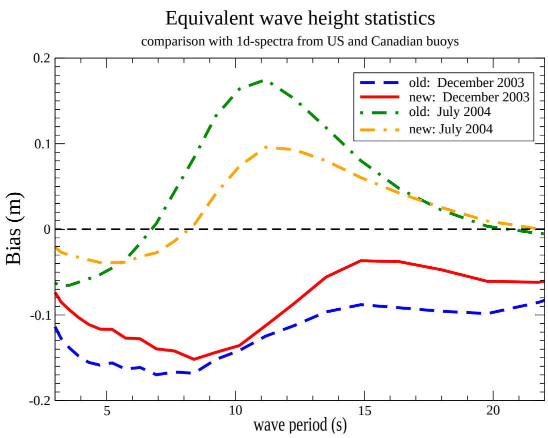

(c) BIAS(model-buoy)

Figure 10: Comparison between wave model hindcasts with the new and the old formulation and 1-D wave spectra for locations along the American and Canadian coasts for December 2003 and July 2004. The spectral data were smoothed by averaging over 3 concecutive wave model frequency bins and converting the average energy density to equivalent wave heights. The different statistics are then plotted in terms of the corresponding wave period of each wave model frequency bin at mid point. All runs used the stand-alone 55km model without any data assimilation. The normalised standard deviation of the difference (STDEV) is computed by normalising with the standard deviation of the observations for each frequency bin.

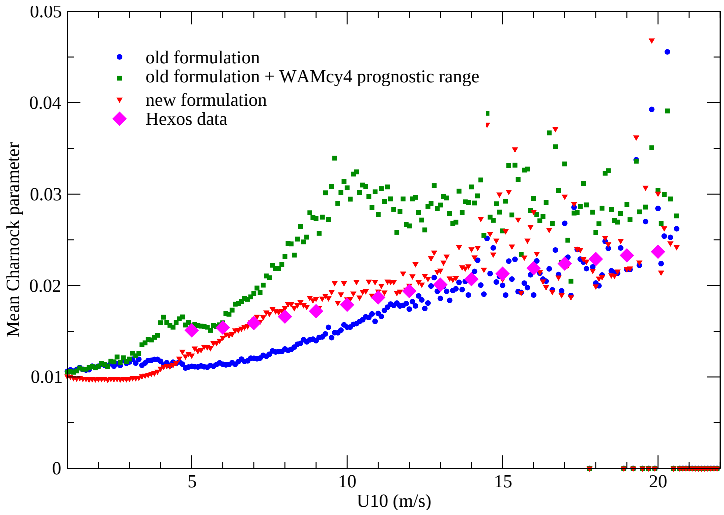

Figure 11: Typical evolution of the mean Charnock parameter as a function of 10m wind speed. The mean value is obtained by averaging all grid point values that are within a given $0.1 m/s$ wind speed bin. Also shown is the relationship between the mean Charnock and the 10m wind speed as derived from the field experiment HEXOS (Smith et al. 1992.)

4.2 Coupled IFS/WAM.

The new formulation is also beneficial on the two-way coupling with the atmosphere. In Fig. 11, the mean Charnock parameter as a function of the 10m wind speed is displayed. As was shown back in 1999, the old formulation with the original WAMcy4 prognostic frequency range had a tendency to return too high Charnock around 10 m/s. This led to the introduction of the current prognostice range. Successive changes to the model have reduced the mean Charnock to levels below the mean typical values as indicated by the HEXOS data (Janssen and Bidlot 2001, Abdalla and Bidlot 2002, Bidlot and Janssen 2003). The new version yields mean levels for the Charnock parameter that are comparable to the mean HEXOS data (Smith et al. 1992.). The mean Charnock is also less noisy for low wind speed around 5 m/s.

With CY29R1, it is now possible to run the new climate package developed by the physical aspects section with the coupling to the wave model. In this configuration, the IFS is run at T95L60 with the 3° wave model for over a year from 3 consecutive starting dates with prescribed analysed SST. Averaging over the 3 realisations and over the last 12 months yields the climate of the model. The change in climate for 10m wind speed is presented in Fig. 12. With the new model formulation, there appears to be a small northward shift of the storm track over the southern ocean and some strenghtening of the winds over a large portion of the northern hemisphere and some weakening over the eastern south Pacific. This climate run also confirms what was found with the stand-alone WAM hindcasts. Namely, wave height is generally increased in the storm tracks (Fig. 13) and decreased in areas which are dominated by swell. The impact of the new formulation on the mean period climate is nicely illustrated in Fig. 14. As expected, T_z is much reduced for a large portion of the tropics and the extra tropics where swell and windsea might be present.

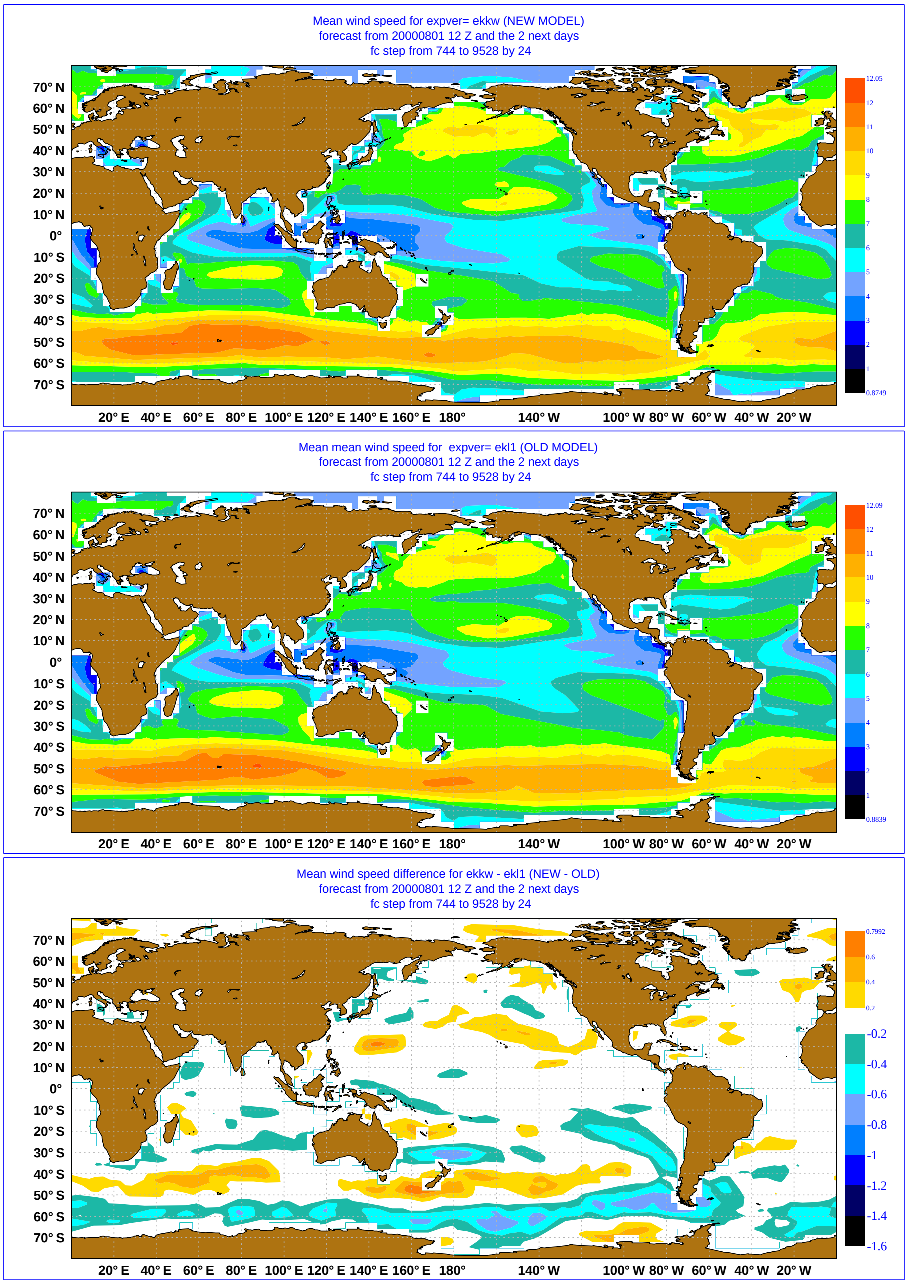

Figure 12: 10m wind speed climate as derived from 3 successive long forecasts at T95L60 coupled to the 3° WAM. The annual mean is shown in the top panel for the new formulation and in the middle panel for the reference run. The difference between the two is shown in the bottom panel (new-old).

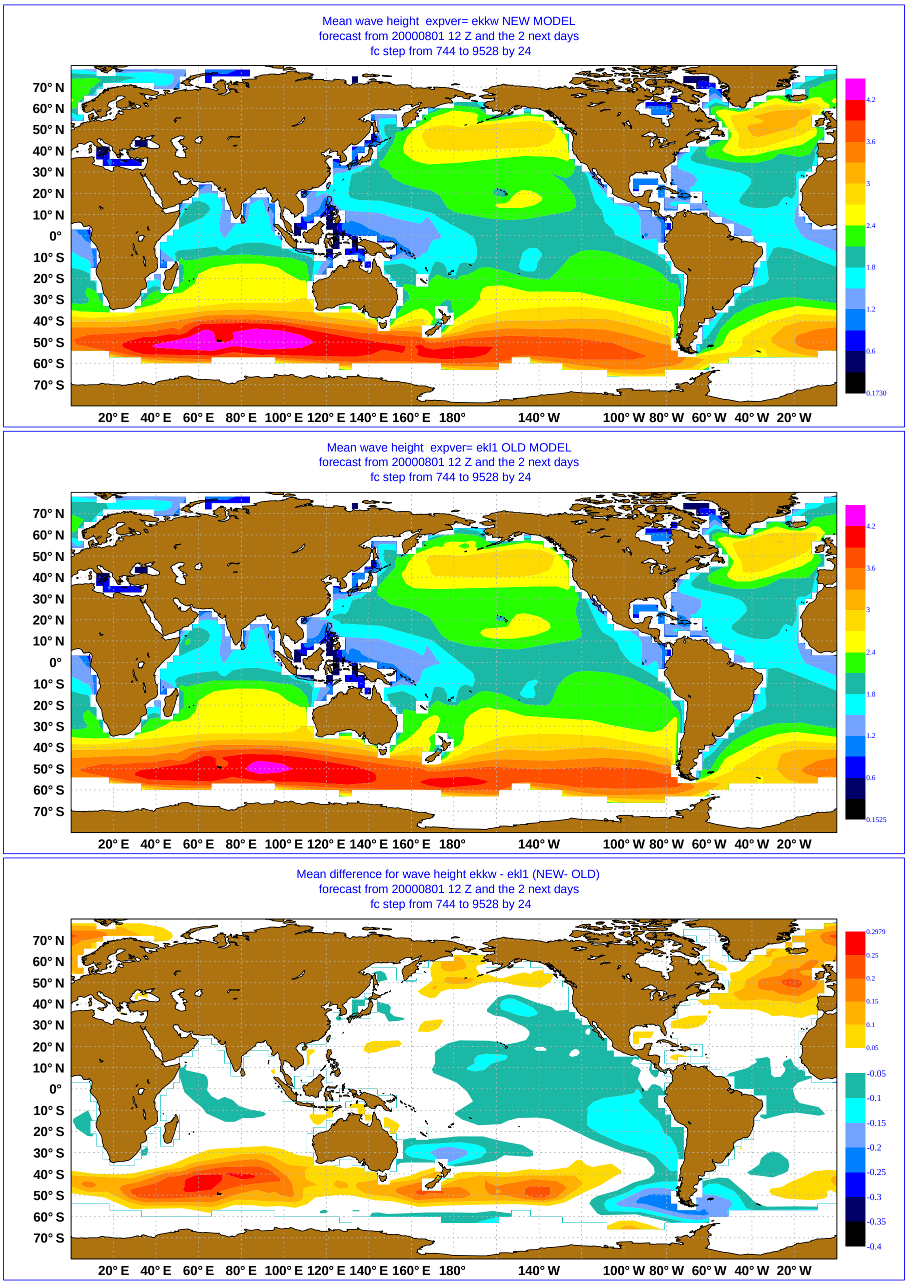

Figure 13: Wave height climate as derived from 3 successive long forecasts at T95L60 coupled to the 3° WAM. The annual mean is shown in the top panel for the new formulation and in the middle panel for the reference run. The difference between the two is shown in the bottom panel (new-old).

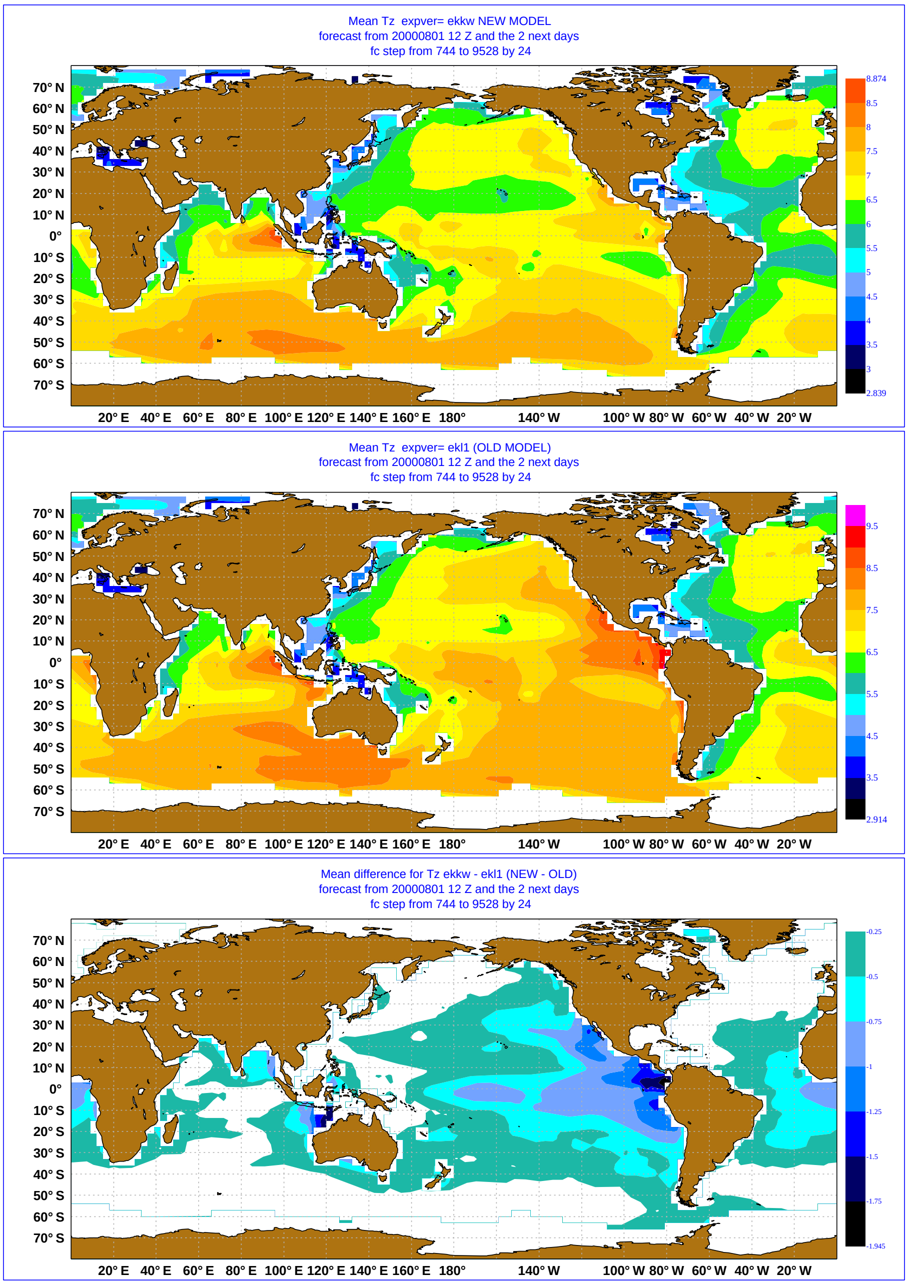

Figure 14: Mean wave period climate as derived from 3 successive long forecasts at T95L60 coupled to the 3° WAM. The annual mean is shown in the top panel for the new formulation and in the middle panel for the reference run. The difference between the two is shown in the bottom panel (new-old).

4.3 Forecast experiments.

The impact of the new formulation on the wave height scores can be isolated by running the stand-alone version of WAM in forecast mode using operational analysis and forecast winds as input. ENVISAT altimeter wave heights were also used to produce the wave analysis. Fig. 15 shows the wave height scores for the northern hemisphere and the tropics for the period from December 2003 to January 2004. The beneficial impact of the new formulation is clearly visible for both the extra tropics (similar results were found for other areas) and the tropics. Verification of the analyses against buoys and Jason yields results that are similar to those previously found in hindcast mode, confirming the global better quality of the analysis obtained with the new formulation. Buoy data can also be used to assess the forecast performance with similar conclusion as above (Fig. 16).

Similar scores were produced for a 2 month period in July-August 2004. When verified against their own analysis (Fig. 17), the new formulation has slightly faster error growth in the extra tropics. This is unfortunate, however it has been shown that the new analysis is better in many respects. If both forecast experiments are compared to the new analysis (Fig. 18), the discrepency between the two is reduced. Nevertheless, in the extra tropics, forecasts from the new system still exibit slightly larger random errors after day 3. This is also supported by the comparison with buoy data (Fig. 16) and with altimeter data (Fig. 19 and 20) (only Jason is shown because its coverage was more global than ENVISAT). By construction, the new formulation is more sensitive to wind forcing, therefore, forecast errors in the wind forcing will result in larger wave height errors.

In coupled mode, the wave model improvements might however also benefit the evolution of the atmosphere. Several coupled experiments were done but the overall impact of the new formulation on the wave model was found to be pretty much similar to that of the stand-alone runs and in line with what has be found in the latest CY29R1 e-suite.

4.4 CY29R1 e-suite.

Fig. 21 and 22 show the wave height and 10m wind scores against own analysis for the northern hemisphere and the tropics. The e-suite wave height random error in the extra tropics is slightly worse but without any significant the degradation of any other statistics. As it was the case in the pre-esuite evaluation, the new analysis was found to have improved with respect to buoy and altimeter data. In the tropics, the scores are fairly neutral apart from a slight loss in correlation. The e-suite wind speed scores are better for the extra tropics but not in the tropics.

Scores with respect to the new better analysis are presented in Fig. 23 and Fig. 24 for wave height and wind speed respectively. With this new analysis as reference, e-suite wave height scores are slightly better for short range forecasts and fairly neutral for longer forecast range. This is also true when forecasts are compared to buoy data (Fig. 25) and against altimeter data (Fig. 26 and 27) as well. Fig. 24 shows that wind speed scores are also a bit better as a whole.

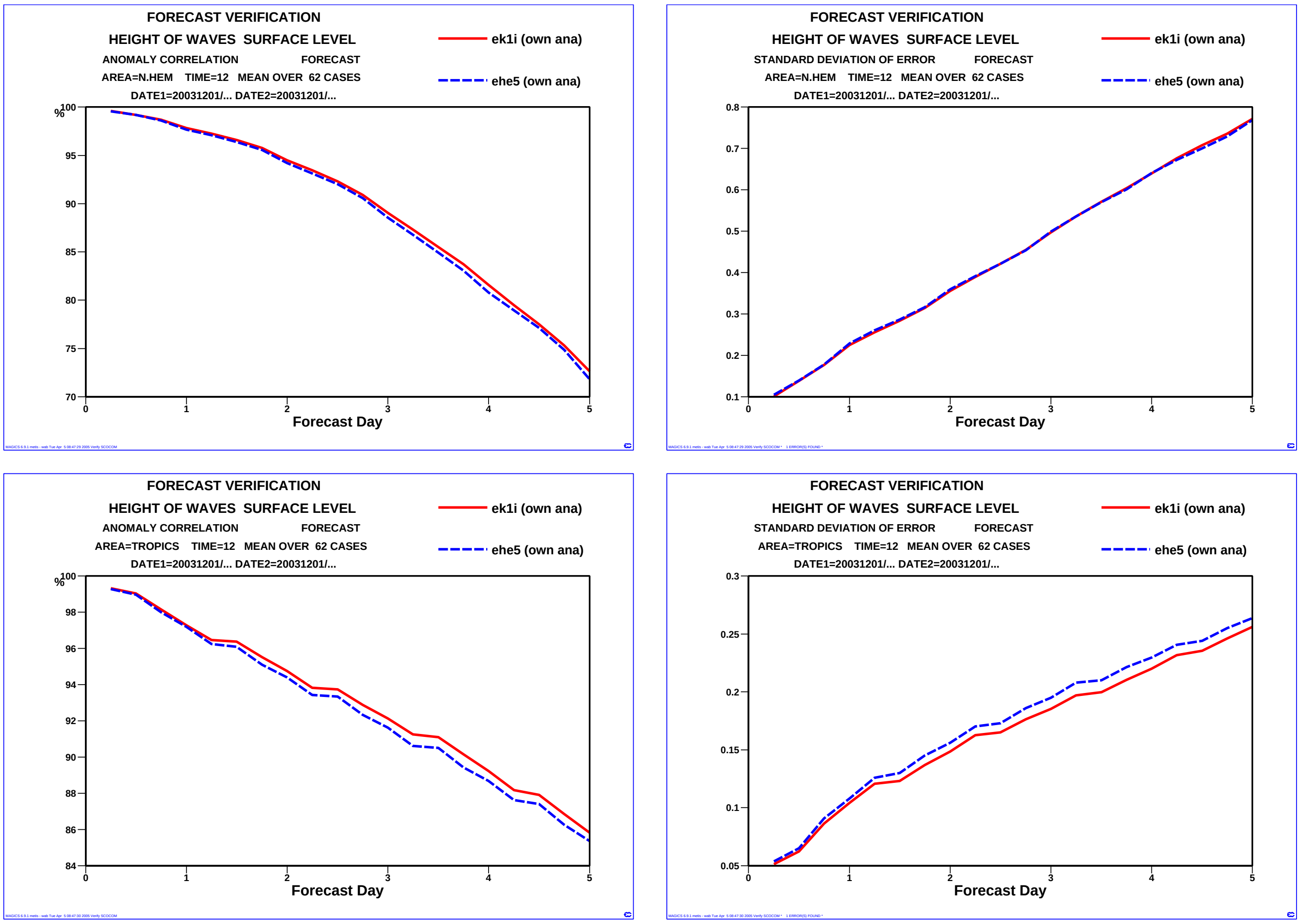

Figure 15: Wave height scores for the stand-alone WAM in winter (Dec 03-Jan 04) against own analysis. E-suite wind fields (expver=10, e-suite at the time) were used and ENVISAT altimeter wave heights were assimilated. The new formulation (ek1i, solid red cuves) is compared to the old version (ehe5, dash blue curves). Note the unusual display of 6 hourly scores.

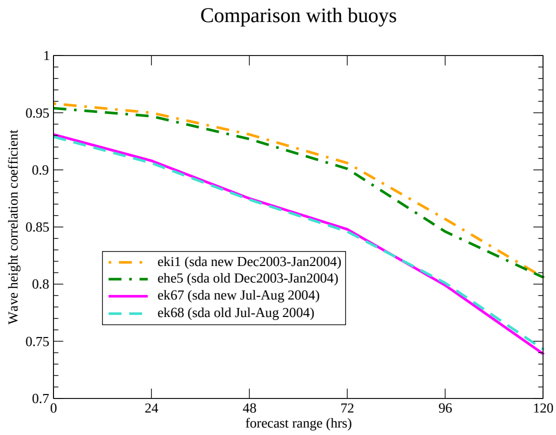

(a) CORRELATION COEFFICIENT

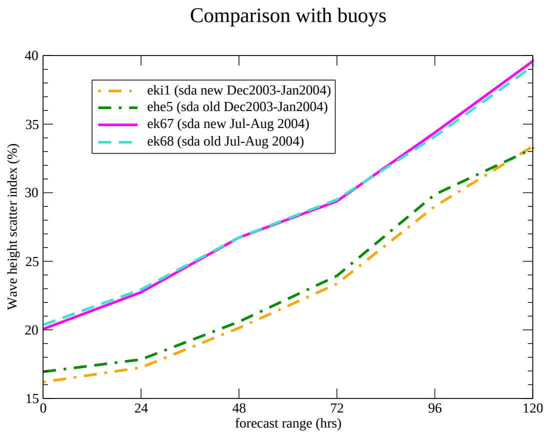

(b) SCATTER INDEX

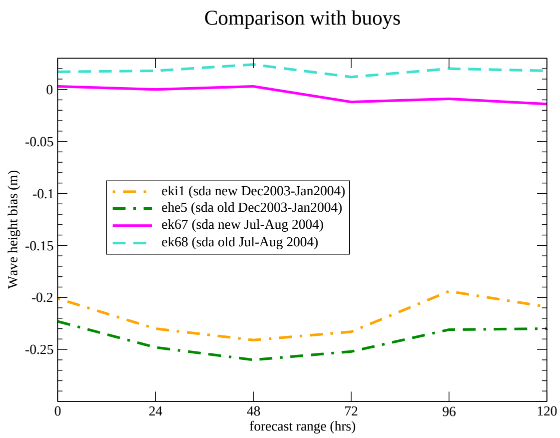

(c) BIAS

Figure 16: Comparison between wave height forecasts and buoy data for pairs of experiments comparing the new formulation with the old. Forecasts scores obtained with the stand-alone WAM setup with the new formulation (eki1, orange dot-dash curve) and the reference (ehe5, green dash-dot curve) are shown for the period of 1^{st} December 2003 to 31^{th} January 2004. Similarly for the period from 1^{st} July to 31^{th} August 2004 (new ek67, solid magenta curve and old ek68, dash turquoise curve). Only forecasts from 12Z are considered.

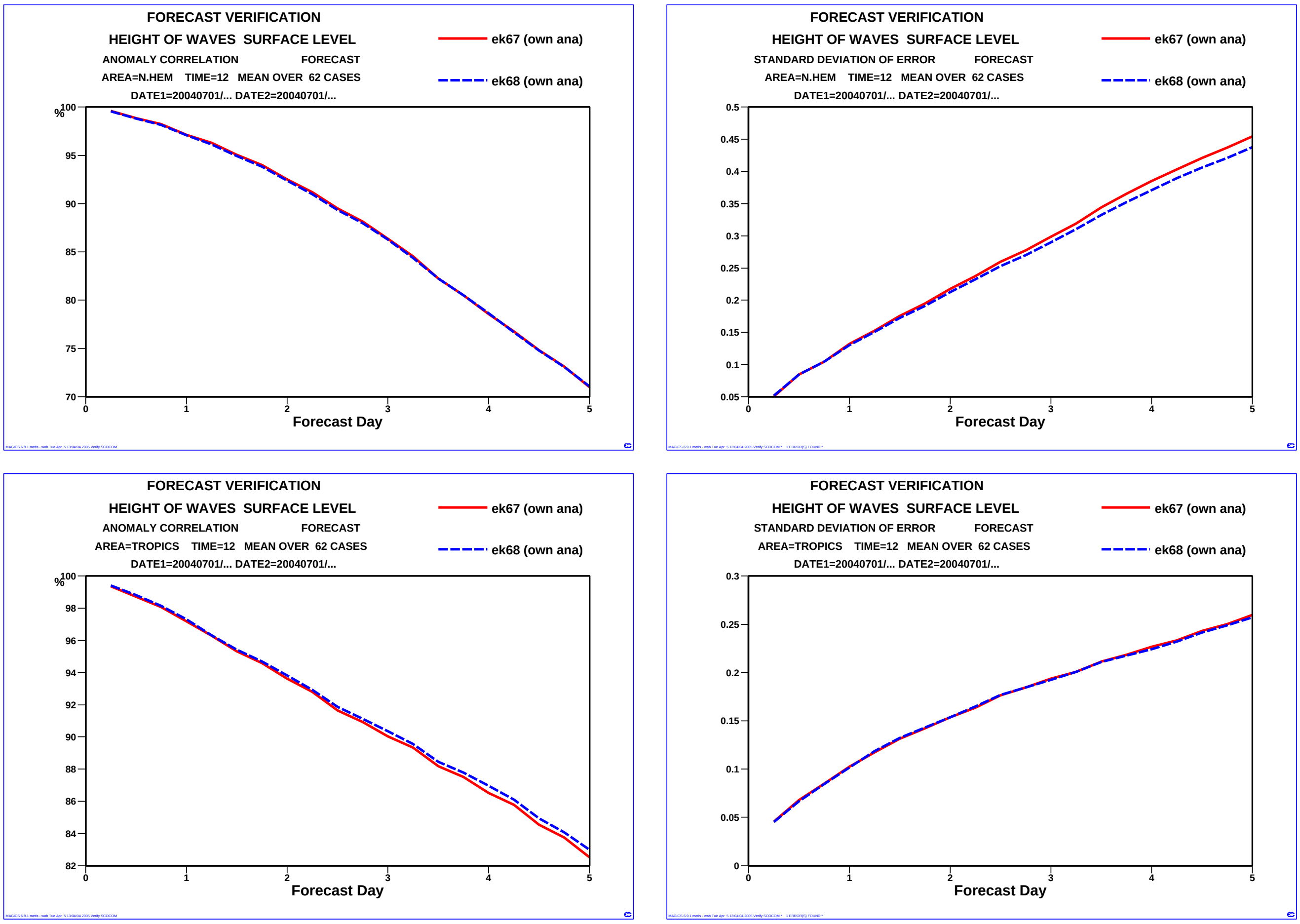

Figure 17: Wave height scores for the stand-alone WAM in summer (July-Aug 04) against own analysis. Operational wind fields (expver=1) were used and ENVISAT altimeter wave heights were assimilated. The new formulation (ek67, solid red cuves) is compared to the old version (ek68, dash blue curves). Note the unusual display of 6 hourly scores.

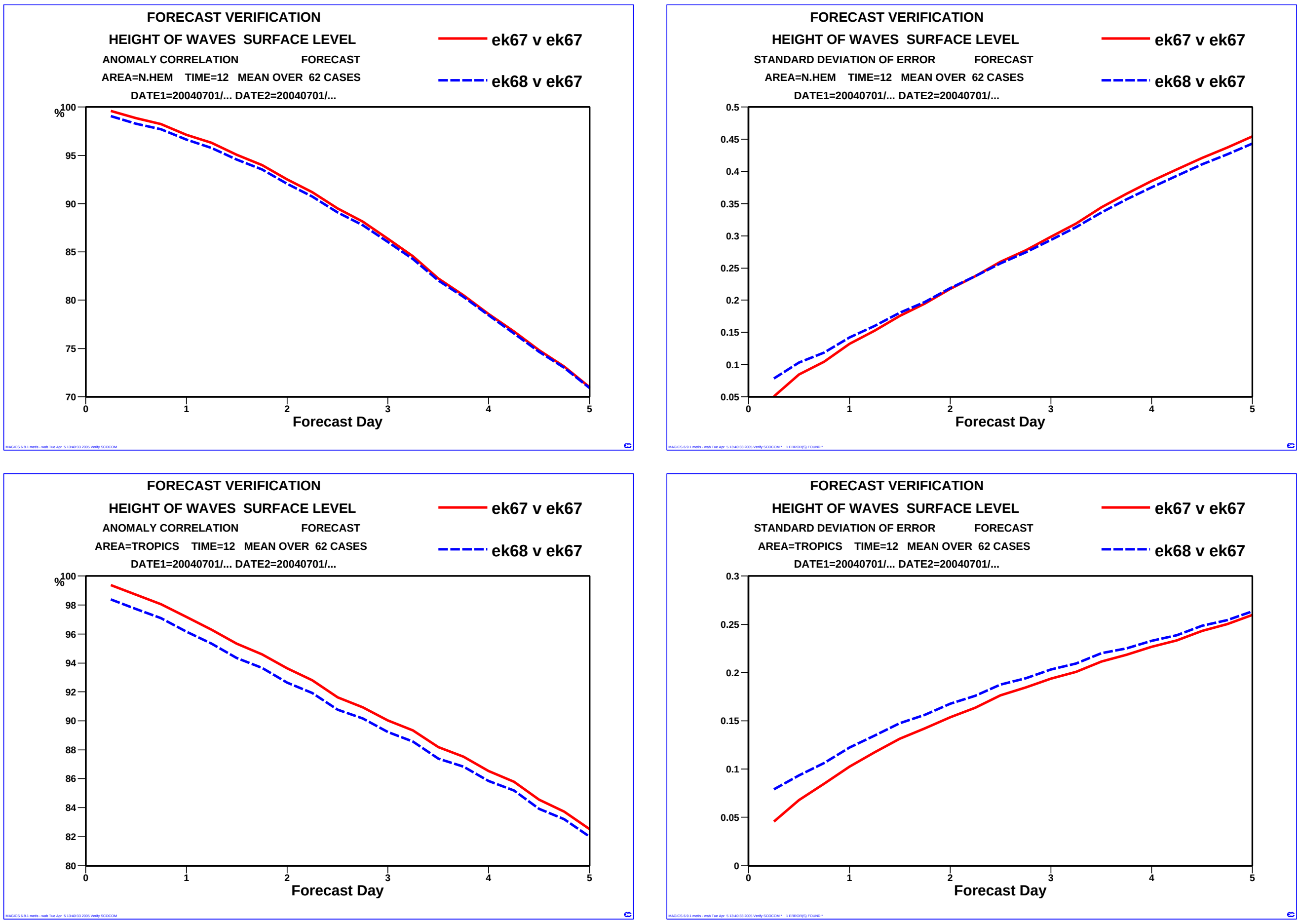

Figure 18: Wave height scores for the stand-alone WAM in summer (July-Aug 04) against new analysis (ek67). Operational wind fields (expver=1) were used and ENVISAT altimeter wave heights were assimilated. The new formulation (ek67, solid red cuves) is compared to the old version (ek68, dash blue curves). Note the unusual display of 6 hourly scores.

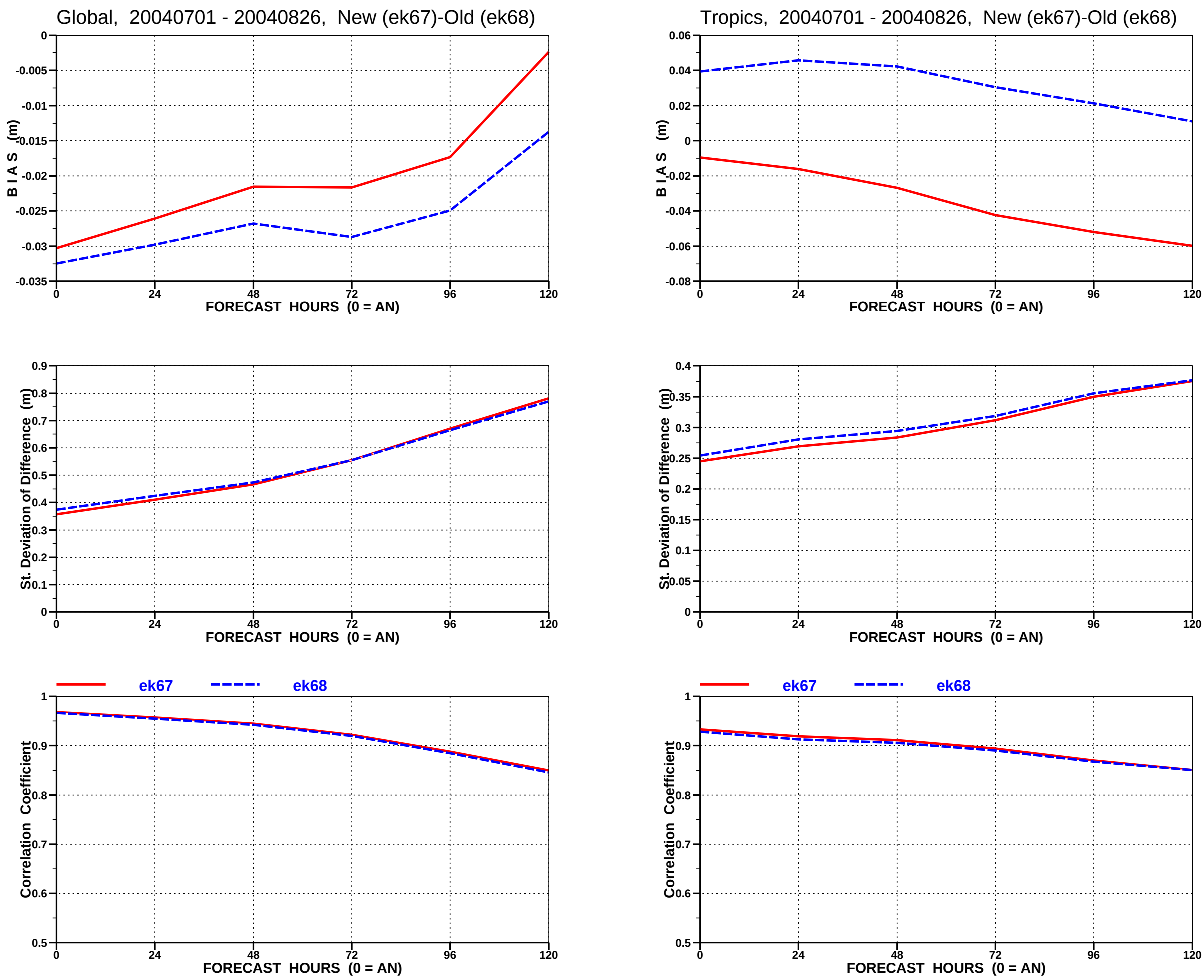

(a) global

(b) tropics

Figure 19: Wave height scores against Jason wave height data for July and August 2004. Solid red curves are for the new formulation (ek67) whereas dash blue curves are for the reference (ek68). Quality controlled Jason data were reduced by 4% and were averaged over the model grid. Tropics are defined as the area between ±20°.

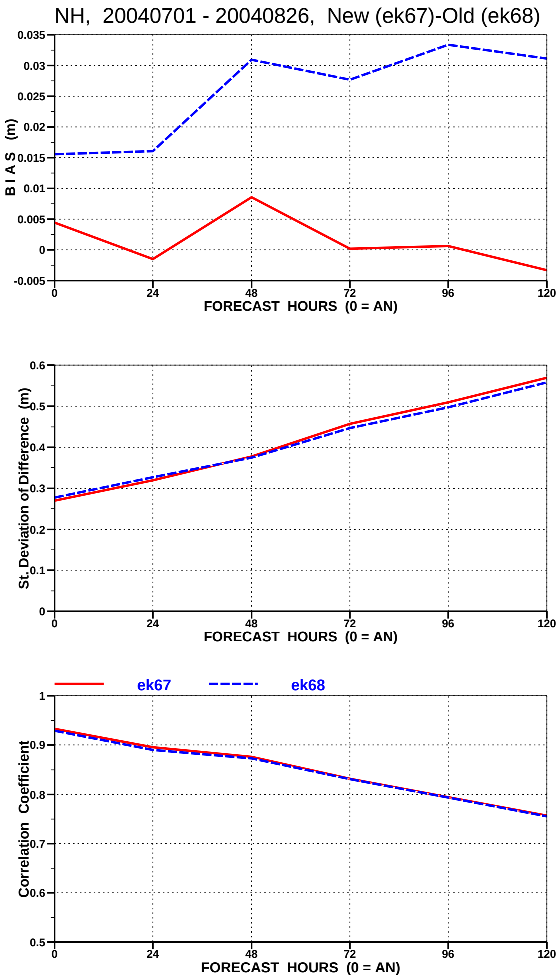

(a) Northern hemisphere

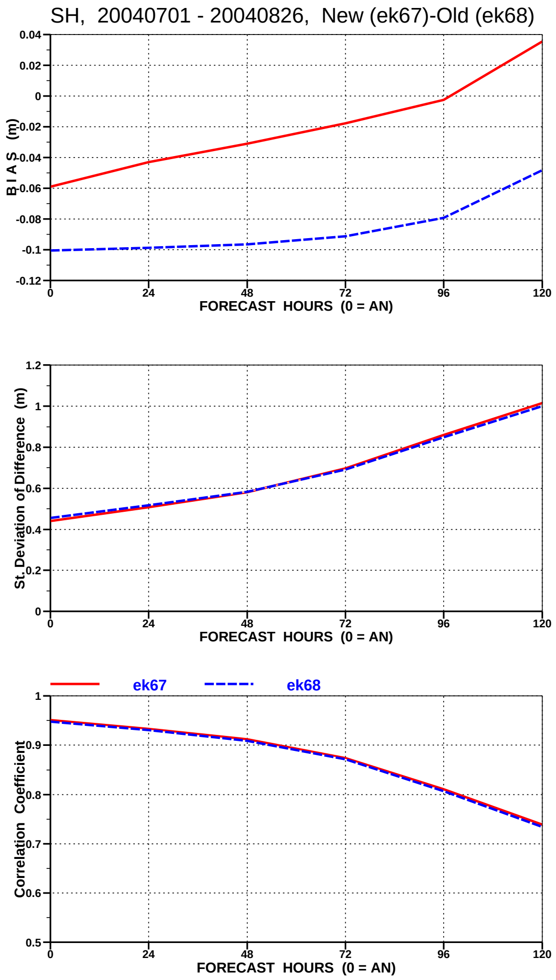

(b) Southern hemisphere

Figure 20: See Fig. 19

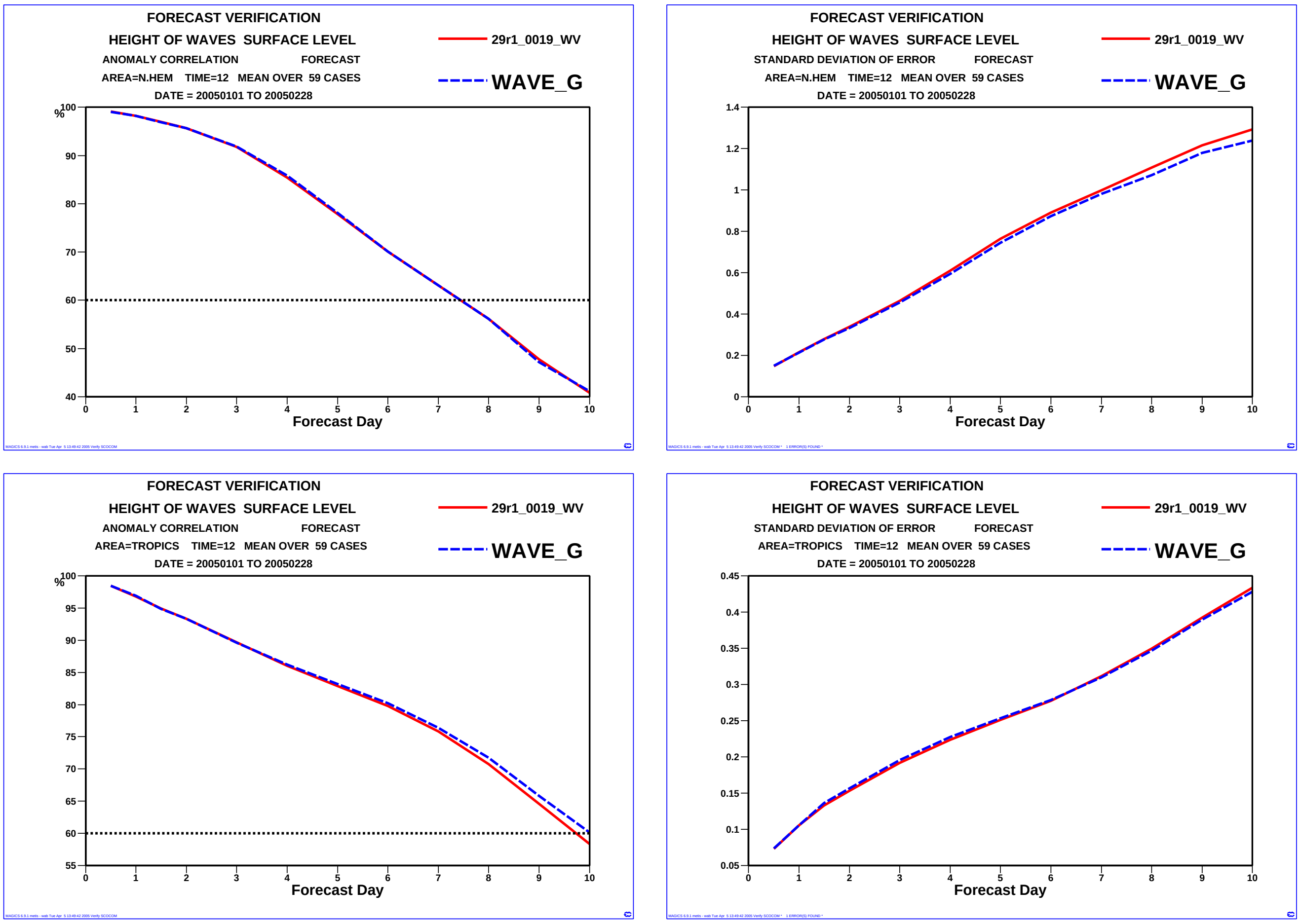

Figure 21: Wave height scores for the CY29R1 e-suite against own analysis for January and February 2005. Solid red curves are for the CY29R1 e-suite whereas dash blue curves are for the o-suite.

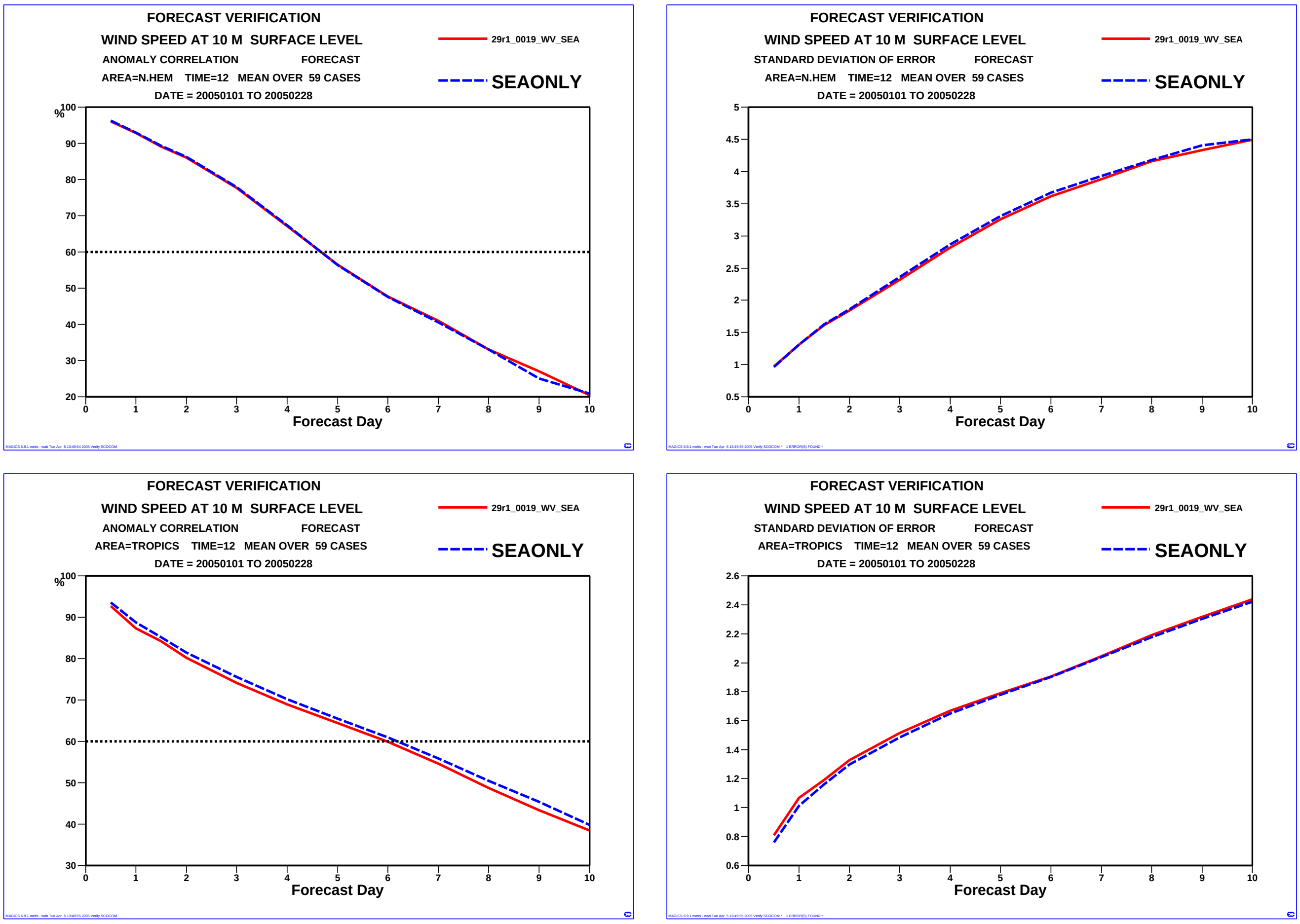

Figure 22: Wind speed scores for the CY29R1 e-suite against own analysis for January and February 2005. Solid red curves are for the CY29R1 e-suite whereas dash blue curves are for the o-suite.

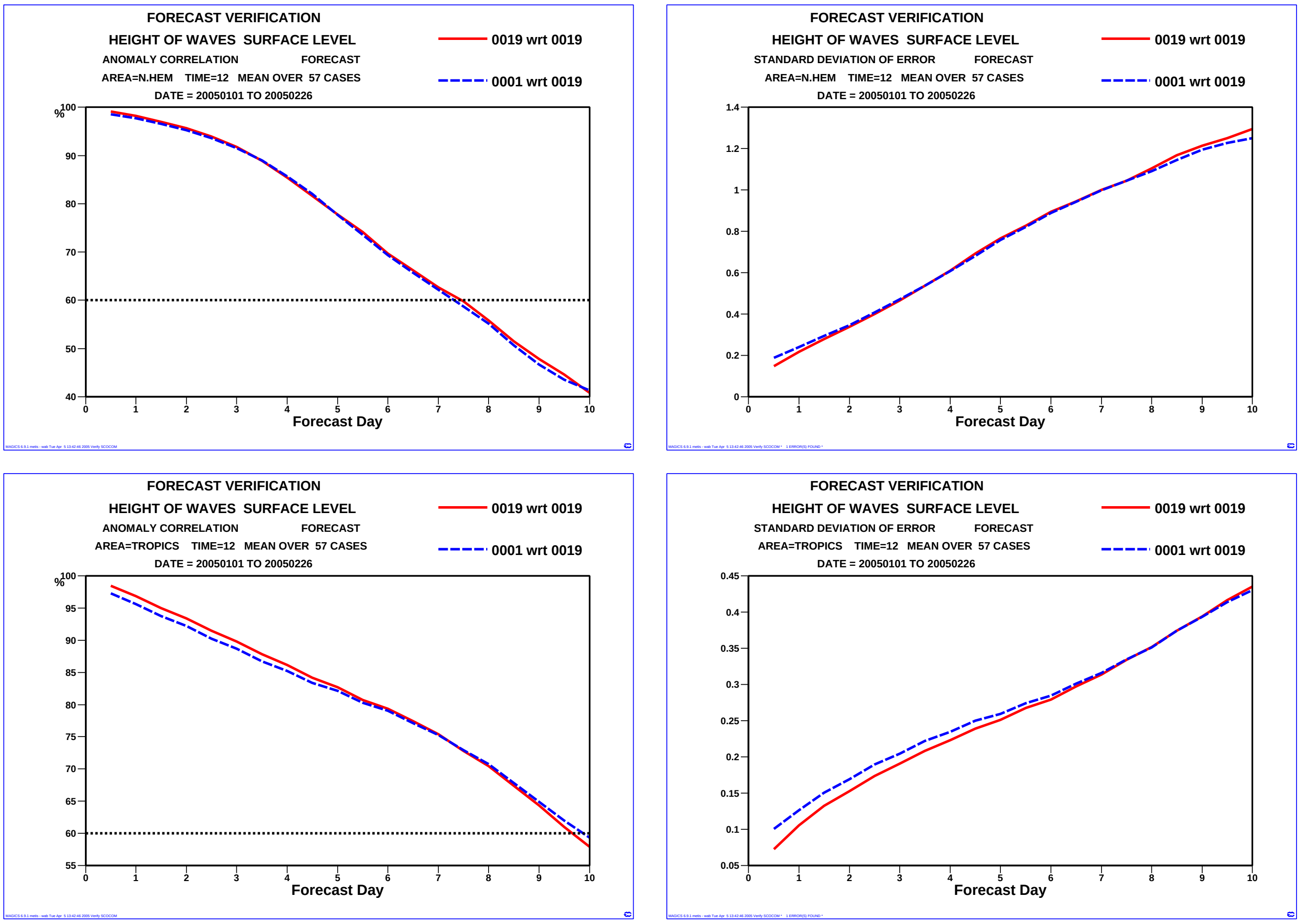

Figure 23: Wave height scores for the CY29R1 e-suite against e-suite analysis for January and February 2005. Solid red curves are for the CY29R1 e-suite whereas dash blue curves are for the o-suite.

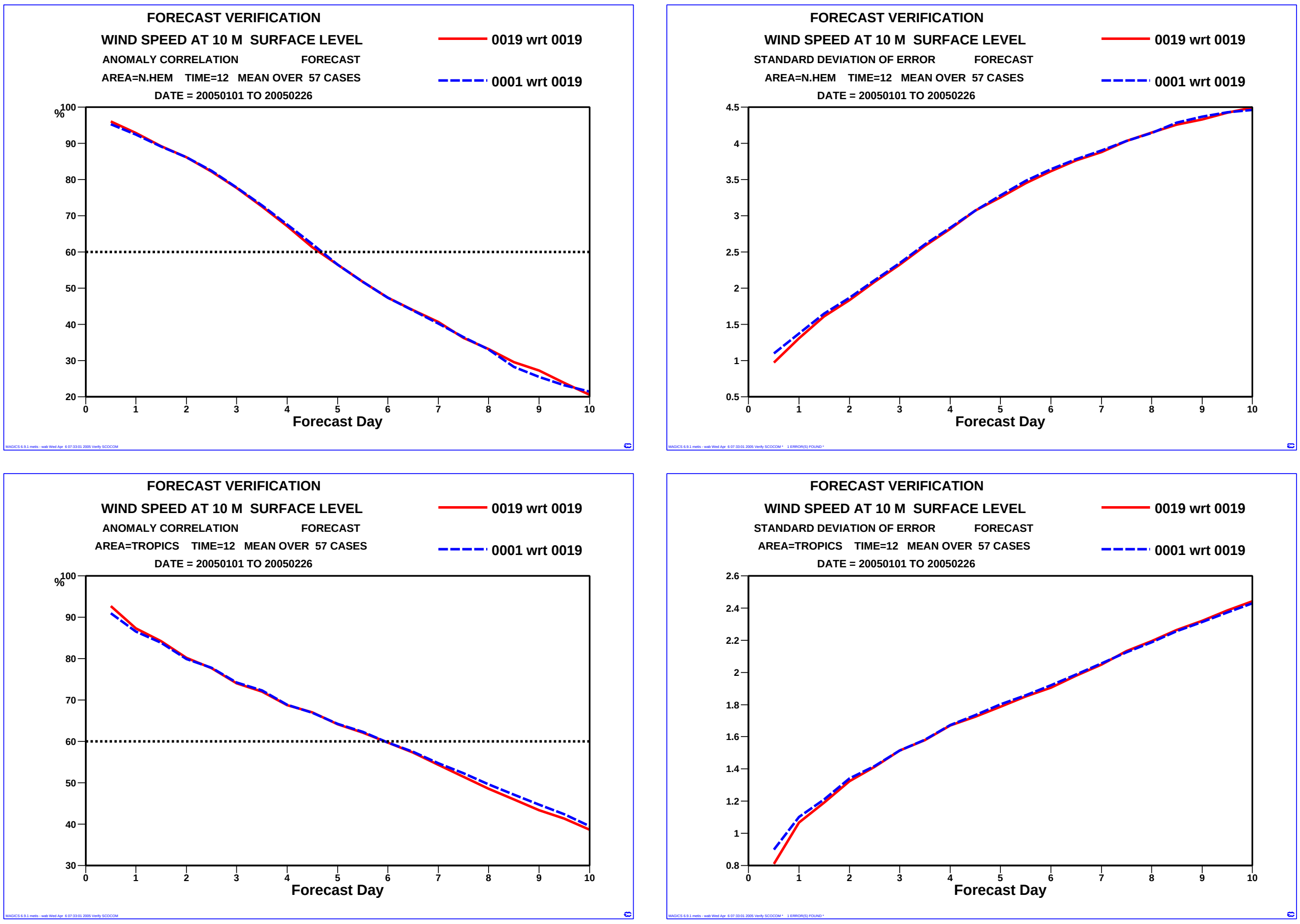

Figure 24: Wind speed scores for the CY29R1 e-suite against e-suite analysis for January and February 2005. Solid red curves are for the CY29R1 e-suite whereas dash blue curves are for the o-suite.

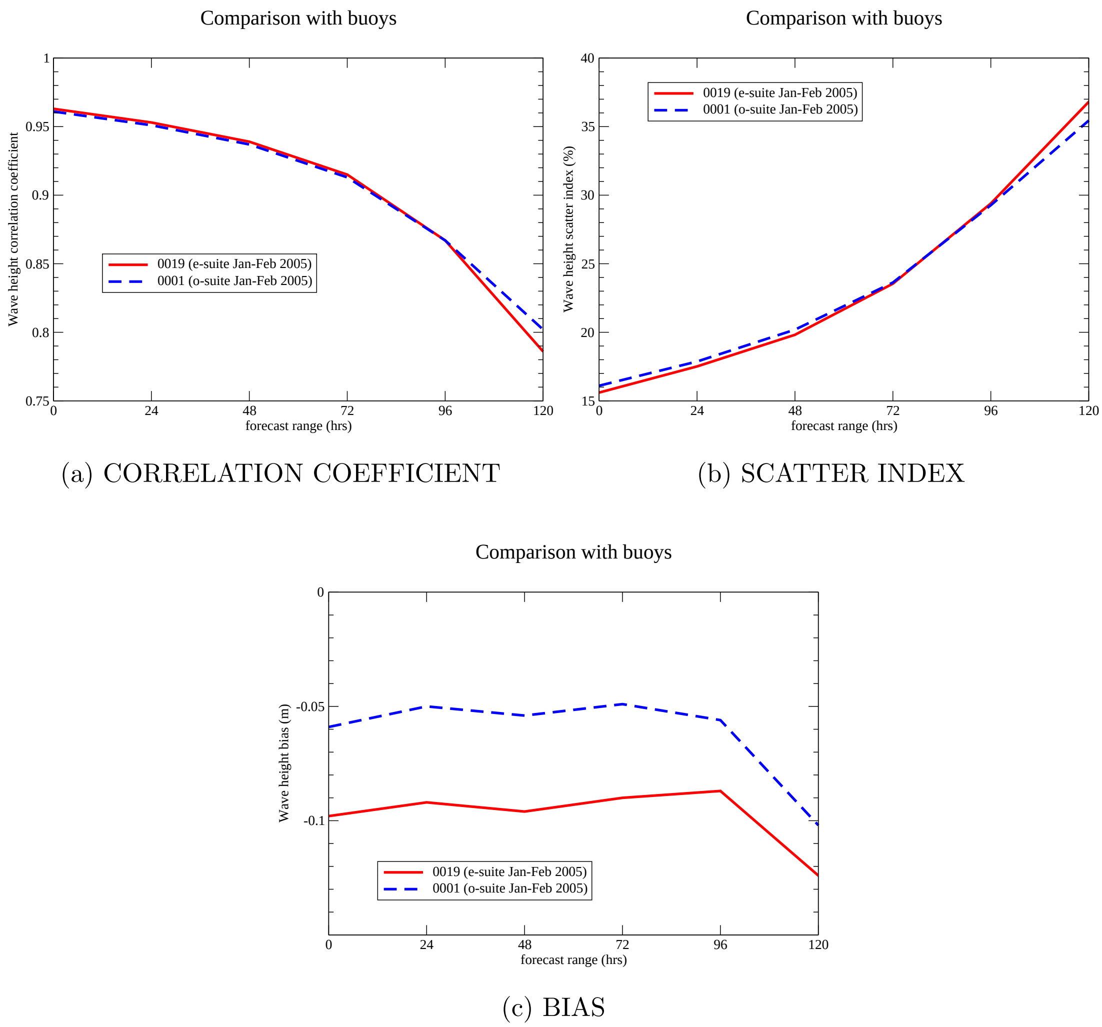

(a) CORRELATION COEFFICIENT

(b) SCATTER INDEX

(c) BIAS

Figure 25: Comparison between wave height forecasts and buoy data comparing the new formulation with the old. Forecasts from the CY29R1 e-suite (0019, red solid curve) are compared to the o-suite (0001, blue dash curve) for the 0 and 12Z forecasts combined from January 1^{st} to February 28^{th} 2005.

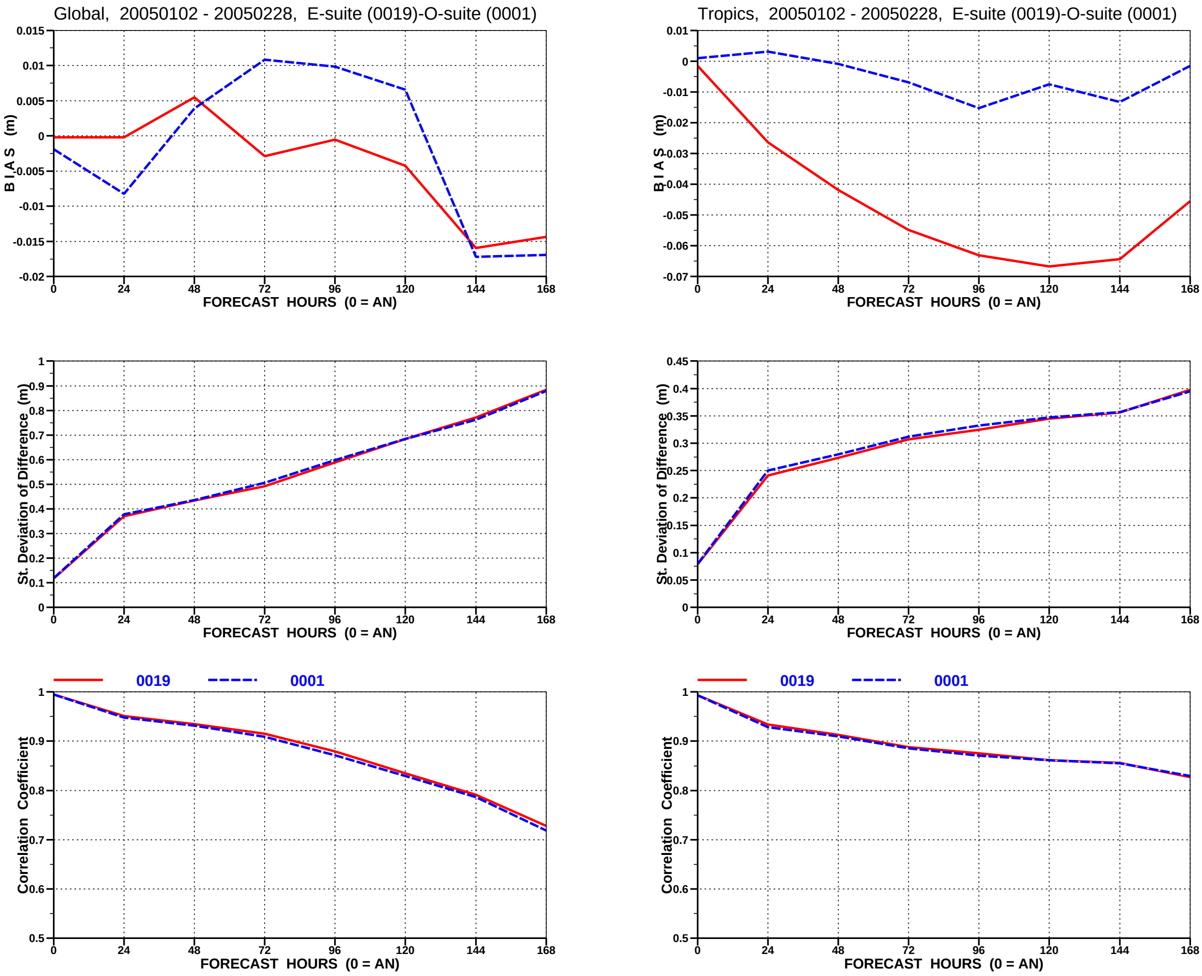

(a) global

(b) tropics

Figure 26: Wave height scores against ENVISAT wave height data for January and February 2005. Solid red curves are for the CY29R1 e-suite whereas dash blue curves are for the o-suite. Quality controlled ENVISAT data were reduced by 4% and were averaged over the model grid. Tropics are defined as the area between ±20°.

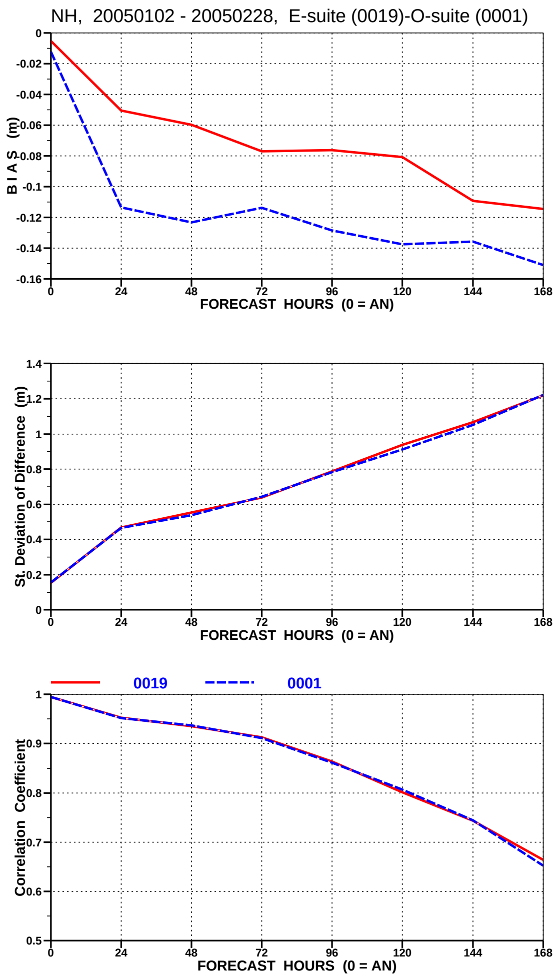

(a) Northern hemisphere

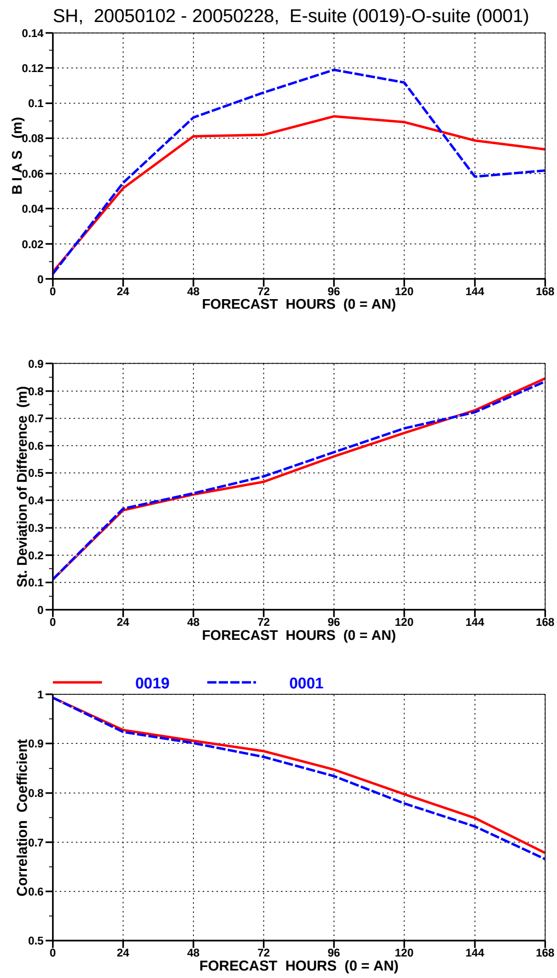

(b) Southern hemisphere

Figure 27: See Fig. 26

4.5 Indian buoy data

Oceanor had reported a problem with the centre's wave period when compared to buoy data they had obtained from the National Institute of Ocean Technology in India. At the time, we could not carry out a similar comparison because we could not get access to the data. However, since October 2004, wind and wave data from buoys deployed around India have become freely available on the GTS (as dribu data). Only 3 hourly data are available, nevertheless, a comparison of the o-suite and e-suite analyses with the data shows the remarkable improvement both in terms of wave height and mean period in e-suite.

Comparison with Indian buoy data - S.I.(%) [bias]		
data source	o-suite	e-suite
H_s GTS (m)	29.2 [0.08]	26.4 [0.08]
T_z GTS (s)	29.7 [1.40]	13.8 [-0.10]
wind speed GTS (m/s)	25.6 [-0.27]	25.8 [-0.28]

Table 3: Comparison with Indian buoy data for January and February 2005. The o-suite is compared to the e-suite in terms of scatter index (standard deviation of the difference normalised by the mean of the observations) and bias (model-buoy) for wave height (H_s), mean period (T_z) and wind speed. The buoy data were obtained from the operational archive (GTS) for locations in the Arabian Sea and the Bay of Bengal.

5 Conclusions.

In CY29R1, a new wave model configuration was introduced in order to better represent the interaction between windsea and swell. It was achieved by using a modified definition of the mean wave steepness and mean frequency in the formulation for the dissipation source term that puts more emphasis on the high frequencies. Generally, the impact of the new formulation and the associated changes to the wave model is positive for the analysis and the short range forecasts, especially for parameters that are most sensitive to the high frequency part of the wave spectrum such as the mean wave periods. For longer forecast range, however, the benefit of the new formulation in the extra tropics is less clear. Standard scoring method based on its own analysis hint at a small degradation mostly in terms of random error. However, comparison against buoy and altimeter data and scores based on the improved analysis from new model setup indicate a small improvement.

References

Abdalla, S. and J. Bidlot, 2002. Wind gustiness and air density effect and other key changes to the wave model in CY25r1. Memorandum Research Department R60.9/SA/0273.

Bidlot, J. and P. Janssen, 2003. Unresolved bathymetry, neutral winds and new stress tables in WAM (main contribution to CY28R1). Memorandum Research Department R60.9/JR/0400.

Hasselmann, K. 1974. On the spectral dissipation of ocean waves due to whitecapping. Boundary Layer Meteorol. 6, 107-127.

Hersbach, H. and P.A.E.M. Janssen, 1999. Improvement of the short-fetch behavior in the wave ocean model (WAM). J. Atm. Ocean. Techn., 16, 884-892.

Janssen, P. and J. Bidlot, 2001. Impact of revised surface roughness calculation on mini vorticices (CY24R2). Memorandum Research Department R60.9/PJ/44.

Janssen, P. 2004. The interaction of ocean waves and wind. Cambridge: Cambridge University Press.

Komen, G.J., K. Hasselmann and S. Hasselmann, 1984. On the existence of a fully developed windsea spectrum. J. Phys. Oceanogr. 14, 1271-1285.

Komen, G.J., L. Cavaleri, M. Donelan, K. Hasselmann, S. Hasselmann, and P.A.E.M. Janssen, 1994. Dynamics and Modelling of Ocean Waves. Cambridge: Cambridge University Press.

Kumar, R., D. Stammer, W.K. Melville, P. Janssen, 2003. Electromagnetic bias estimates based on TOPEX, buoy, and wave model data. J. Geophys. Research, 108, 3351,doi:10.1029/2002JC001525.

Pierson, W.J.,Jr and L. Moskowitz, 1964. A proposed spectral form for fully developed wind seas based on the similarity theory of S.A. Kitaigorodskii. J. Geophys. Res. 69, 5181.

Smith, S.D., R.J. Anderson, W.A. Oost, C. Kraan, N. Maat, J. DeCosmo, K.B. Katsaros, K.L. Davidson, K. Bumke, L. Hasse and H.M. Chadwick, 1992. Sea surface wind stress and drag coefficients: the HEXOS results. Boundary Layer Meteorol. 60, 106-142.

Snyder, R.L., F.W. Dobson, J.A. Elliott and R.B. Long 1981. Array measurements of atmospheric pressure fluctuations above surface gravity waves. J. Fluid Mech., 102, 1-59.